Tufts University
Department of Biology

Senior Honors Thesis

Live Cell Phase Imaging Under Whole Blood Shear Flow Using Oblique Back-Illumination

By
Diana Mojahed

Submitted in partial fulfillment of the requirements for
the degree of Bachelor of Science in 2016

Acknowledgements

There are countless people who have been instrumental in fostering my undergraduate research career and for making this work a success.

I am eternally grateful to Dr. Gary Tearney for providing me with the opportunity to work in your lab and for being a role model for my aspiring career as a physician-scientist and for instilling in me a great passion to pursue graduate and medical studies in this field.

First, I would like to thank my mentor, Dr. Tim Ford, for teaching me all that I know about oblique back-illumination microscopy (OBM) and for providing feedback on my designs. Thank you for your countless hours of mentorship on not only optics but also the importance of resourcefulness. I am grateful that you fostered my curiosity about OBM since the time I first noticed your work on a wireless implantable microscope in BAR-805.

Thank you to former Tearney lab mentors, Dr. Kengyeh Chu and Dr. Carolin Unglert, for building the foundations of my knowledge of optical imaging at the Tearney lab and for fostering my young interest in biomedical optics research and medicine. Thank you to all the members of the Tearney lab for your mentorship, advice, and friendship and for making my time at the Tearney lab a pleasure and lifelong memory. It is because of you all and your contagious dedication to fascinating research that I am always excited to come to the lab.

Thank you to Dr. Ana Pardo and Dr. Vladmir Vinarksy of the Rajagopal lab for providing me with several vials of 3T3 endothelial cells and offering cell culture tips and tricks, which were instrumental in getting our cell culture started. Thank you to Emma Briars of the Hasan Lab for allowing me to store my frozen cells in their liquid nitrogen tank in the absence of other alternatives.

Thanks to my lab colleague and friend, Paul Dannenberg, for performing experiments with me at MGH when my OBM setup still needed two people to operate and for listening to Taylor Swift on repeat with me to keep up the morale while performing experiments (nothing encourages success like the song *Style*).

Thank you to Dr. Mohini Lutchman, my office mate and one of my all-time most trusted confidantes, for encouraging me through the toughest of times and reminding me to "chill out" every now and then.

Thanks most of all to my parents, Hiam and Mahmood, my closest friends (Jamie, Mark, Sasha, Amanda), and my love Tom Mason for their unwavering love and support and for always encouraging me to pursue my passions.

Thank you to my favorite library, Tisch Library at Tufts University, which has been the center of my studying and for providing a comfortable place for me to work over these past four years.

Thank you to my committee members, Dr. Tim Ford, Professor Harry Bernheim, and Professor Sergio Fantini for their mentorship, advice, and evaluation of this thesis.

Abstract

Understanding the cellular interactions between endothelial cells (EC) and immune modulators is important in understanding immune tolerance in transplantation medicine and biology. Current optical imaging modalities used to observe these interactions include Zernike phase contrast (PC) and differential interference contrast (DIC) microscopy which have limited performance when imaging ECs under physiological whole blood flow conditions due to unfavorable optical properties of erythrocytes. Oblique back-illumination microscopy (OBM) provides high-contrast phase-gradient images of near-surface structures with such strongly scattering backgrounds. In this project we used OBM for imaging ECs under physiological flow and shear conditions first using a simple Ibidi flow chamber, and then translating the design to a fully-integrated BioFlux platform for our collaborators (Pierson Lab at University of Maryland Medical Center in Baltimore, MD).

The imaging setup was comprised of a commercial inverted microscope outfitted with a pair of optical fibers delivering strobed illumination from light-emitting diodes (LEDs) in the red and near-infrared (NIR) spectrum. 3D-printed fiber guides were designed, fabricated, and mounted to a 10× phase contrast objective to position the optical fibers in a range of positions and incidence angles. OBM, PC, and brightfield images of a monolayer of adherent cells under physiological whole blood flow conditions were obtained. The influence of illumination fiber incidence angle, fibers separation, flow chamber depth, and illumination wavelength on OBM image quality were assessed.

Zernike phase contrast microscopy cannot image through more than approximately 10 μm of whole blood due to high optical scattering and absorption. In contrast, we have shown in this work that OBM produces high-quality images of adherent cells and red blood cells

(RBCs) under 5 dynes/cm^2 shear stress and 0.3 – 18 mL/min blood flow in commercial flow chambers of heights 70 – 800 μm. Based on our results, we believe OBM could be adapted for use in commercial chambers for imaging of monolayers with highly scattering backgrounds.

Table of Contents

Chapter 1 Introduction

Understanding the mechanisms of immune injury to and chronic rejection of organ transplants aids in the prevention of rejection and promotion of immune tolerance following transplantation. Complications in transplant medicine begin at the host blood-donor tissue endothelial interface. Optical microscopy is a well-suited tool for monitoring cellular interaction at this interface, but is impractical for *in vivo* applications (Zavislan, 2009). Accordingly, an *in vitro* imaging technique is sought for monitoring cell interactions in physiological whole blood conditions. Blood is mostly composed of red blood cells, which are highly scattering and absorptive, making it difficult to image into blood for most microscopy techniques (Yurkin, et al., 2005). The purpose of this study was to develop and validate oblique back-illumination microscopy (OBM) for imaging endothelial cells under whole blood shear flow in a commercial flow chamber. First, a setup was designed for the simple and inexpensive commercial Ibidi flow chamber and then, upon successfully designing a setup of OBM that could image endothelial cells and neutrophils in a whole blood perfusion sample, translating the design for the fully-integrated BioFlux flow chamber platform at the Pierson lab at the University of Maryland Medical Center in Baltimore, MD.

1.1 Xenotransplantation

Over 120,000 patients in the United States are in need of an organ transplant because they are suffering from end-stage organ failure (American Journal of Transplantation, 2016). However, there are only approximately 15,000 organ donors and less than 30,000 transplants performed each year (American Journal of Transplantation, 2016). This shortage of donor organs

restricts allotransplantation significantly. Alternative sources of organs are being sought to narrow the gap between demand for organs and the supply of them.

One of the alternatives being considered is the xenotransplantation of organs from genetically modified pigs (Klymiuk, Aigner, Brem, & Wolf, 2010). Currently there are several issues, including immune rejection, that must be dealt with before xenotransplantation can be a viable option for humans (Ekser, et al., 2012). Wild type (WT) porcine organs are rejected in humans because human antibodies interact with the porcine galactose α-1,3-galactose (Gal) antigen and consequently cause injury to endothelial cells, thrombosis, and ultimately hyperacute rejection of donated organs (Harris, et al., 2015). The Gal antigen has been inhibited in certain pigs, α-1,3-galactosyl-transferase knockout (GalTKO), and their organs have been observed to survive longer when transplanted to non-human primates, notably baboons (Burdorf, et al., 2014). Further, transgenic introduction of human proteins, such as the complement regulatory protein GalTKO.hCD46 (CD46), markedly improves organ survival (Ekser et al., 2012). CD46 prevents the host cell from being attacked by complement-mediated damage and promotes T-cell activation (Kickler, et al., 2012).

Although organ survival is improved, thrombosis remains a major contributory factor for acute and chronic rejection of organs and a critical hurdle for xenotransplantation as a technique. Being able to implement xenotransplantation in the future requires thorough mechanistic understanding of thrombus formation (Harris, et al., 2015).

Xenotransplantation researchers have limited tools to study the mechanism of thrombus formation *in vitro* under physiological conditions. It is necessary to observe these interactions at the cellular because whole organ studies, despite their translational and clinical relevance, look at multiple pathways simultaneously, none of which may be fully understood and it is difficult to

isolate specific interactions. Insight at this level would facilitate an understanding of the complex nature of these cellular interactions. Here we propose the use of dynamic physiological shear-flow *in vitro* to help with a functional dissection of these interactions.

1.2 Shear-Flow Assays

To model the endothelial cell-blood interactions, assays must be performed under dynamic conditions because static assays lack the physiologic characteristics of blood flow through vasculature (Schroeder, et al., 2005). Additionally, to model these interactions, the surfaces of the platform must be coated with confluent endothelium, rather than ligand-coated surfaces, which have been previously studied but do not accurately represent physiology and limit translation (Prabhakarpandian, Shen, Pant, & Kiani, 2011). A typical plate flow chamber consists of an inflow well, which flows into a perfusion channel, and subsequently flows to an outflow well. The bottom of the channel is tissue-culture treated to allow for adhesion of a monolayer. A perfusion pump is connected to both ends of the chamber to induce shear flow, and the perfusate is not recirculated. The plate is placed on the stage of an inverted microscope for imaging and analysis. The bottom of each channel is made with a coverslip for optimal imaging.

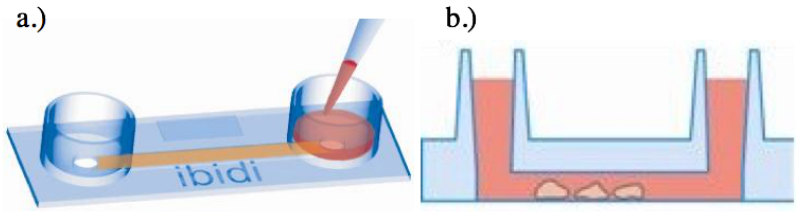

Figure 1. Overview of the Ibid flow chamber system. a.) The Ibidi flow chamber consists of an inflow and outflow well, to which a pneumatic pump is attached on either end via Luer lock connections. Connecting the two wells is a central channel, in which the monolayer is seeded and flow is induced. b.) Sketch of the cell monolayer seeded in the flow channel. Perfusate flows over the monolayer (Ibidi USA).

Fluxion Biosciences, Inc. (San Francisco, CA) and Ibidi, GmbH (Planegg, Germany) have developed widely used commercial flow chambers. The Ibidi flow chamber is the simpler,

cheaper option that was the focus of the first half of this work (Figure 1 and Chapter 2).

A channel runs along the Ibidi plate with an inflow and outflow well at either end of the channel, where perfusate enters the channel. The bottom of the channel is tissue-cultured treated for growing a monolayer. There is no heating capability and the flow must be induced by a separate perfusion pump.

The BioFlux platform (Fluxion Biosciences) is a fully-integrated, high-end instrument for performing controlled flow channel assays and provides physiological shear flow conditions for live cell flow assays. The system includes an inverted microscope, low-shear microfluidic plates, a heating element, and a pneumatic pressure controller (Figure 2).

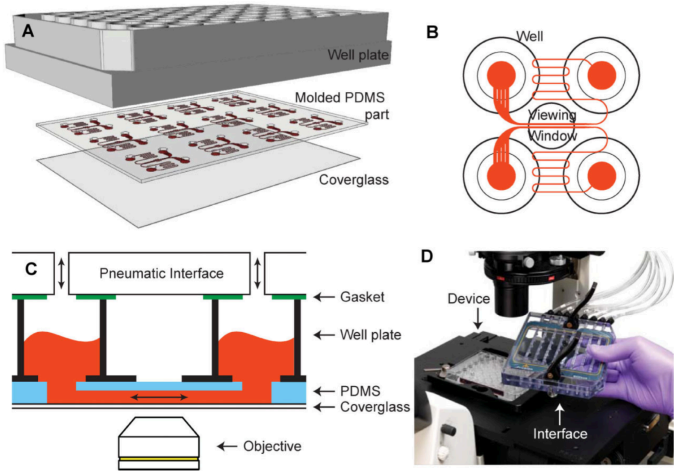

Figure 2. Overview of the Bioflux System. A.) The Bioflux system utilizes a well plate interface, in which cells are seeded and flow is induced. The bottom of the plate is covered with a #1.5 borosilicate glass coverslip for optimal imaging. B.) The well plate interface is equipped with flow cells, in which the monolayer is seeded, and perfusate is loaded with a pipette. C.) Cross-sectional area of each flow channel. Bioflux controller is attached to the inflow and outflow wells and perfusion is induced. Shear and flow rate is controlled based on desired characteristics. D.) The flow chamber system is imaged using a Zeiss Z1 Axio Observer inverted microscope. (Conant, et al., 2011)

1.3 Background on Microscopy Techniques

1.3.1 Confocal Microscopy

Confocal microscopy (Figure 3) is a well-established optical imaging technique that provides optical sectioning and rejection of out-of-focus background signal. A confocal microscope contains illumination and detection optics. Illumination of the sample is provided by a tightly focused spatially coherent light source, which is known as the critical illumination. Unlike widefield microscopy, which detects the signal from a wide field of the sample, confocal microscopy only detects the signal from the area of critical illumination, and rejects signals from out-of-focus planes. The overlap of the illumination volume and detection is known as the probe volume, and is confined in both lateral and axial directions (Mertz, 2009).

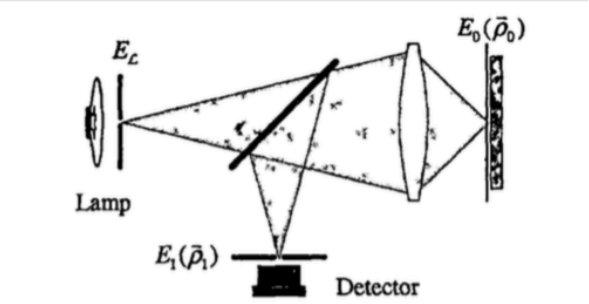

Figure 3. Reflection geometry of a confocal microscopy. The illumination pinhole produces a tightly focused beam that illuminates the probe volume, and the detection pinhole restricts detection to reflections from the probe volume. Images of the x-y focal plane are produced by a scanning mechanism (not shown) (Mertz, 2009).

The signal from a confocal microscope is limited to a small probe volume, and this volume must be scanned over a large area in order to build up an image. In order to scan over a large area of a sample, laser-beam steering is most commonly implemented. Galvanometer mirrors tilt the illumination beam, which translates the probe volume across the sample x-y plane. In order to scan through the z-plane, images must be acquired at different focal depths by axially translating the condenser lens or sample to produce a 3D stack (Mertz, 2009). This is the

rate-limiting step of confocal microscopy because the scanning speed determines image acquisition speeds (Callamaras & Parker, 1999). Thus, confocal microscopy is a slow and expensive technique, but has the advantage of high axial resolution and high quality optically sectioned images of a sample, such as a cell monolayer.

Confocal microscopy can be operated in either reflection or transmission configurations (Mertz, 2009). Reflectance mode is convenient because the same optics can be used for both illumination and detection, while the galvanometer scanning mirrors can both scan the illumination beam in one direction and then descan the detection beam in the reverse direction. However, the penetration depth is limited by loss of the excitation energy throughout the beam path, so this configuration is limited when imaging through scattering or absorbing media, such as whole blood, as would be in the case of an *in vitro* flow chamber (Cox & Sheppard, 2004). Confocal microscopy could be used to image the surface layer of a channel with whole blood flow, but not through the entire volume of the channel.

Thrombus formation has been studied using custom-made flow chambers and the BioFlux platform and in combination with confocal microscopy. Specifically, neutrophil aggregation in the process of thrombus formation was imaged with and without coagulation using a custom-made flow chamber (Van Kruchten, Cosemans, & Heemskerk, 2012). Additionally, confluent human umbilical vein endothelial cells (HUVEC) were grown in BioFlux microfluidic channels (Fluxion Biosciences) and monocyte-accumulation and monocyte-detachment assays were performed (Mukovozov, et al., 2015). For the attachment assays, the goal was to monitor the number of leukocytes that interacted with the monolayer. For the detachment assays, the number of monocytes that remained adherent to the monolayer was observed after a period of incrementally increasing shear force. Their data show that after the

monocyte-accumulation assays, monocytes that were treated with Slit treatment, which inhibits monocyte adhesion, monocytes adhered significantly less than untreated monocytes. The most important takeaway from the results is that only the monocytes, which were stained with Calcein AM (which stains cells with nuclei), were visible in the images, not the monolayer itself (Figure 4).

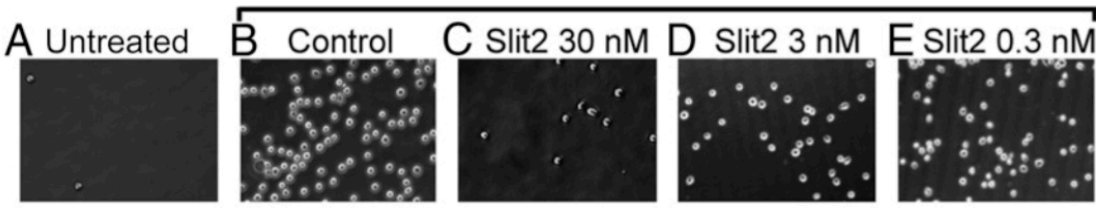

Figure 4. Confocal images of monocyte adhesion after performing monocyte adhesion assay under various conditions. a.) No monocytes in assay, b.) Monocytes in assay without Slit treatment, which is known to inhibition monocyte adhesion, and c-d) different concentrations of Slit treatment. Cells were imaged using a Leica DMIRE2 spinning disc confocal microscope (Mukovozov, et al., 2015).

1.3.2 Widefield Fluorescence Microscopy

Fluorescence microscopy is an imaging technique where contrast is not based on light scattering, but on light absorption (Huang, Bates, & Zhuang, 2009). A sample is illuminated and photon energy is absorbed by fluorescent molecules. Rather than simply being lost as heat, this energy is reemitted as light of a longer wavelength, which is known as fluorescence emission. The intensity of the fluorescence signal is measured by a camera after being spectrally filtered from the excitation signal.

Fluorescence imaging has been used for observing thrombosis (stained neutrophils) and it can image through the depth of the channel, unlike confocal microscopy, but fluorescence requires staining to observe neutrophils and the resulting images are not high resolution. In one study, whole blood was perfused over an endothelial cell monolayer to observe neutrophil adhesion using fluorescence microscopy with BioFlux system (Conant, et al., 2011). Images were acquired using an inverted microscope (Nikon TS100) and charge-coupled device (CCD)

camera (QImaging). The BioFlux software was used to process the fluorescence intensity. Whole blood was treated with Calcein AM before perfusion over HUVEC (Figure 5). Once again, only the neutrophils were visible in these experiments and the HUVEC monolayer was not visible, so interactions between the neutrophils and monolayer could not be observed, and the quality of the images of the neutrophils was low and blurred.

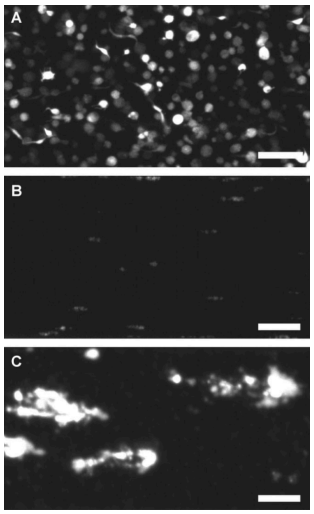

Figure 5. Neutrophil aggregation imaged using fluorescence microscopy. A-C shows various treatments to increase or decrease aggregation. Scale bar 100 μm (Conant, et al., 2011)

The Pierson group at the University of Maryland Medical Center performed a similar experiment and the endothelium was once again not visible, only neutrophil aggregation could be imaged, and thus the interaction between perfusate and monolayer could not be observed. This further illustrates the limitations of fluorescence microscopy for this application (Harris, et al., 2015) (Figure 6).

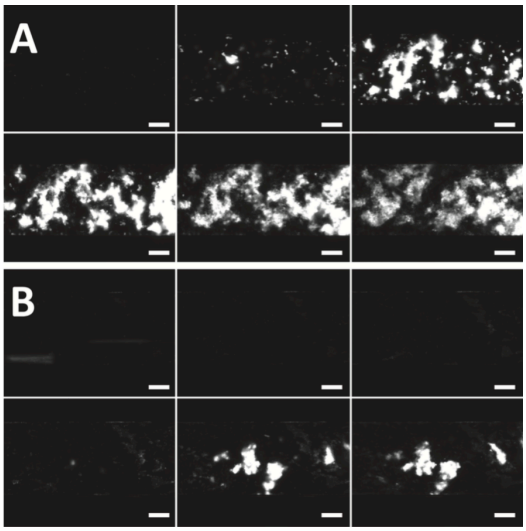

Figure 6. Xenothrombosis on A) wild type (WT) and B) GalTKO monolayer. GalTKO reduces neutrophil aggregation and adhesion, which leads to less collective thrombosis. Images acquired at 0, 10, 20, 30, 40 and 50-minute intervals (left-to-right by row). Scale bar 100 μm (Harris, et al., 2015)

1.3.3 Zernike Phase Contrast Microscopy

Zernike phase contrast microscopy is an optical imaging technique to improve the contrast of unstained objects that would appear transparent in brightfield (Mertz, 2009). One advantage of Zernike microscopy is that specimens can be examined in their natural state without staining or fixation. The technique relies on converting the phase shifts caused by optical path length differences to amplitude shifts via the interference of resultant light waves, which leads to phase contrast.

The optical path length (OPL) is the product of the refractive index and the geometrical path length between two points in the sample. A light wave traveling one wavelength is said to have traveled 2π in phase. A difference in OPL results in a difference of the number of wavelengths a light wave has traveled, and hence a difference in cumulative phase. If an area of the sample has a higher refractive index than its surroundings, there will be deceleration of the wave, which advances its phase. The resulting wave pattern and interference between waves is described by the principle of superposition.

The essential features of a phase contrast microscope are an annular illumination aperture and a phase ring positioned in the detection aperture (Mertz, 2009). When the illumination field interacts with a scattering sample, the field is split into two components: a weak scattered field that fills the detection aperture and a strong non-scattered field, known as the reference field, that neatly goes through the phase ring. The two fields would normally not produce an interference pattern because the scattered field is naturally 90 degrees out of phase with the non-scattered field. The phase ring is designed to apply a further phase shift to the non-scattered field to allow the fields to interfere. The resulting images display phase contrast because variations in OPL in the sample cause phase delays in the scattered field and different intensities in the interference pattern. Figure 7 shows a comparison of a monolayer imaged with both brightfield and phase contrast illumination.

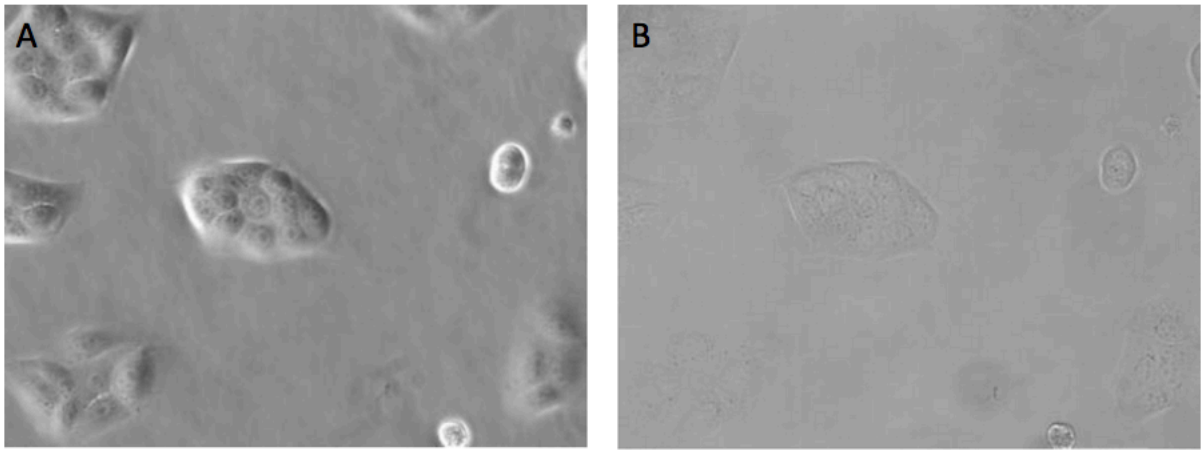

Figure 7. Madin-Darby Canine Kidney (MDCK) cells imaged using (a) Zernike phase contrast microscopy and (b) brightfield microscopy (Ockenga, 2011)

1.3.4 Differential Interference Contrast (DIC) Microscopy

Similar to Zernike microscopy, differential interference contrast (DIC) microscopy is useful for imaging objects that would otherwise be transparent in brightfield (Lang, 1982).

In a transmission configuration, light from a partially-coherent source passes through a polarizer, located under the stage, and then through a Wollaston prism, which splits the beam

into two orthogonally polarized beams traveling along slightly different paths (Figure 8). These two resulting rays are known as the sample and reference rays. Because DIC uses differences in OPL as a source of contrast, it is considered an interferometric technique. The condenser focuses these rays such that they pass through two adjacent points in the sample. The separation allows each ray to experience a difference in OPL where the areas have different refractive indices or difference in optical density, which results in a change in phase of one ray relative to the other. These rays of dissimilar phase are collected by the objective lens and are focused through another Wollaston prism that recombines the rays to produce an interference pattern. The brightening and darkening of the image are based on the OPL difference (Lang, 1982).

The drawbacks of DIC are that the output intensity is a combination of both amplitude and phase contrast so it is difficult to decouple these sources of contrast (Arnison, 2004). An advantage over Zernike is that there is no halo effect in DIC images. However, it difficult to incorporate this into a standard inverted microscope as is the case for Zernike because of the need for Wollaston prisms.

Live cell assays have not been previously imaged using DIC with either the Ibidi or BioFlux systems because DIC is not suitable for imaging through highly scattering media like whole blood because the sample and reference rays become misaligned through scattering and the interference is lost.

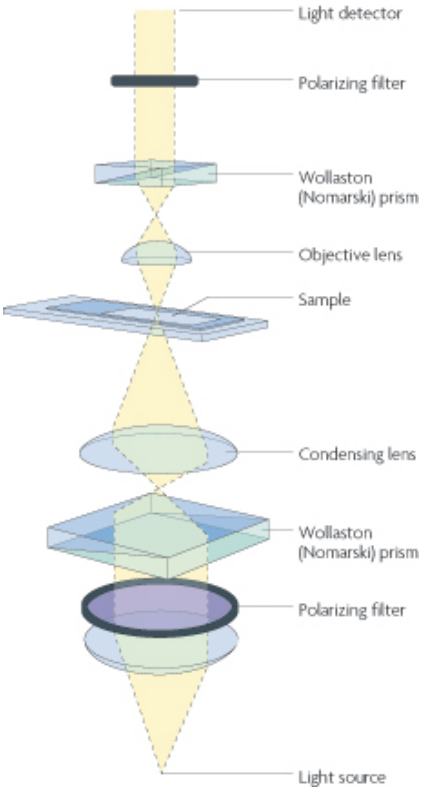

Figure 8. Transillumination configuration of a DIC microscope requires two Wollaston (Nomarki) prisms, a condensing lens, and polarizing filters in addition to standard microscope components (Rosenthal, 2009)

1.3.5 Oblique Back-Illumination Microscopy (OBM)

Oblique back-illumination microscopy (OBM) provides high-contrast phase-gradient images of near-surface structures with strongly scattering backgrounds. OBM leverages the scattering property of blood to redirect the light so it can be detected (Figure 9).

In contrast to phase gradient and DIC imaging, which must be operated in a transillumination configuration, and is therefore limited to use in thin samples, OBM has been demonstrated to work in thick, scattering tissues (Ford et al., 2012). The capability to obtain images through thick, scattering tissues is a key feature for optimizing endoscopic imaging.

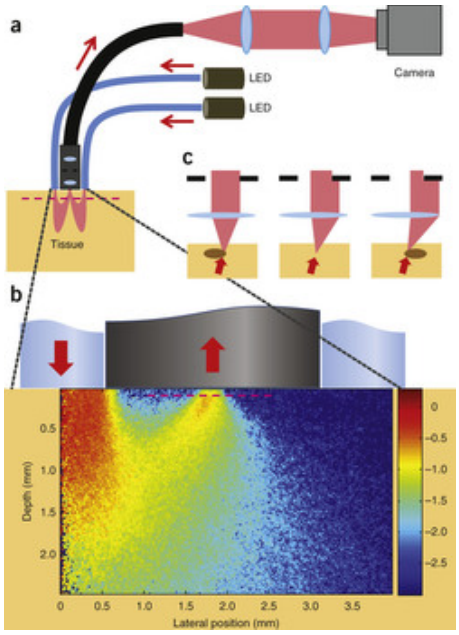

Figure 9. Setup of oblique back-illumination microscopy. (a) Two diametrically opposed LED-coupled optical fibers illuminate the sample, and multiple scattering in the tissue redirects the light to transilluminate the focal plane (magenta line). (b) Density map produced by Monte Carlo simulation. (c) Variation in refractive index at the focal plane leads to phase gradient contrast (Ford, Chu, & Mertz, 2012)

OBM uses illumination that is offset from the detection axis, known as oblique illumination, with diametrically opposed light-emitting diode (LED)-coupled optical fibers. The incident illumination is multiply scattering by the sample (Figure 9), and transilluminates the focal plane. The slope of the variations in refractive index at the focal plane causes a change in intensity, which is the source of phase gradient contrast. Although OBM is in a reflection geometry, Ford aptly explains that it is a "transillumination microscope in disguise" (Ford, Chu, & Mertz, 2012). As with Zernike phase contrast microscopy, OBM image intensity is not only influenced by phase contrast, but also by sample absorption. OBM is unique because it is able to decouple the influence of phase contrast from absorption contrast. It achieves this by sequentially acquiring two images with opposing illumination obliquity and therefore similar values of absorption contrast and opposing values of phase contrast. (Ford, Chu, & Mertz, 2012). These raw images can be added to enhance absorption contrast and cancel out phase gradient contrast, or be

subtracted to enhance phase gradient contrast and cancel out absorption contrast. An example OBM image is displayed in Figure 10.

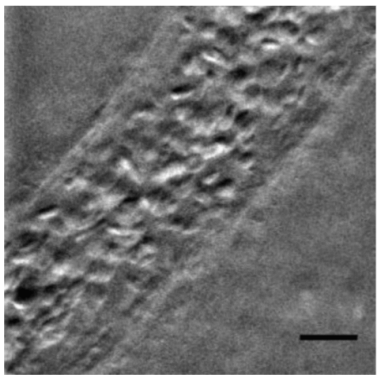

Figure 10. OBM image of blood flow through a post-capillary venule. Scale bar 30 μm (Ford & Mertz, 2013).

1.3.6 Image Quality Metrics

Image quality metrics can be used to determine if an imaging modality is appropriate for an application. The three image quality metrics that were relied on in this study were resolution, contrast, and signal-to-noise ratio (SNR). Image resolution is the shortest distance between two points on an image that can be distinguished as two separate entities (Wang & Li, 1999).

Image contrast, which can colloquially be thought of as "visibility," is defined as signal amplitude divided by background amplitude (for OBM, amplitude is expressed as percent deviation from background, so it is naturally an expression of contrast) (Smith, 2013).

SNR is defined as the amplitude divided by root-mean-squared (RMS) noise fluctuations (Smith, 2013). Simply stated, SNR is the ratio of desired signal to unwanted background noise. SNR is typically measured by taking a short video of a stationary object and pixel-by-pixel dividing the average value by the standard deviation. SNR can be expressed by average SNR (the average of the pixel-by-pixel SNR) or peak SNR (the peak value observed). The most common method is to find the average or peak SNR in a region of interest surrounding a typical cell, for example.

Chapter 2 OBM Setup for Ibidi Flow Chamber

2.1 Introduction

In this second chapter, I will introduce an OBM setup for imaging 3T3 fibroblast cells under physiological flow and shear conditions using Ibidi flow chambers. This work was conducted using the facilities at the Tearney Lab at the Wellman Center for Photomedicine at the Massachusetts General Hospital (MGH). The basis of the work was to validate that OBM could be used as a technique to image a cell monolayer with a highly scattering background in a flow chamber setting.

2.2 Methods

2.2.1 Setup

The OBM setup is shown in Figure 11. OBM was integrated into a standard inverted microscope with a lamp and a camera (Leica DM IL LED), along with a phase ring for Zernike phase contrast to allow for toggling between brightfield, Zernike, and OBM techniques. DIC was not incorporated into this setup because it requires additional components that would be more difficult to toggle between imaging modalities (Lang, 1982). Two diametrically opposed LEDs are coupled into optical fibers (ThorLabs BFH48-1000, 1000 μm core, 0.48 NA, 50 mW, low OH) that are then guided into a 3D-printed device that surrounds a 10× microscope objective (Leica N Plan 10×/0.25 NA) and holds the fibers in place at a fixed angle relative to the optical axis and separation between the ends of the fibers (Figure 12). Three different wavelengths of fiber-coupled LEDs (Thorlabs M660F1, M780F2, M850F2, 660 nm, 770 nm, 850 nm) (Table 1)

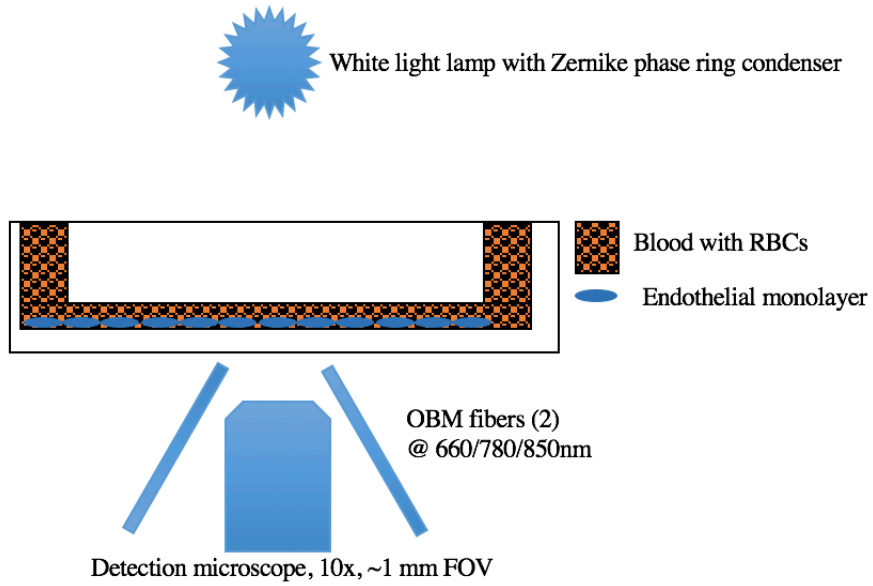

Figure 11. OBM Setup for Leica microscope and Ibidi flow chamber. Can quickly toggle between Zernike, brightfield, and OBM by turning on/off appropriate light sources.

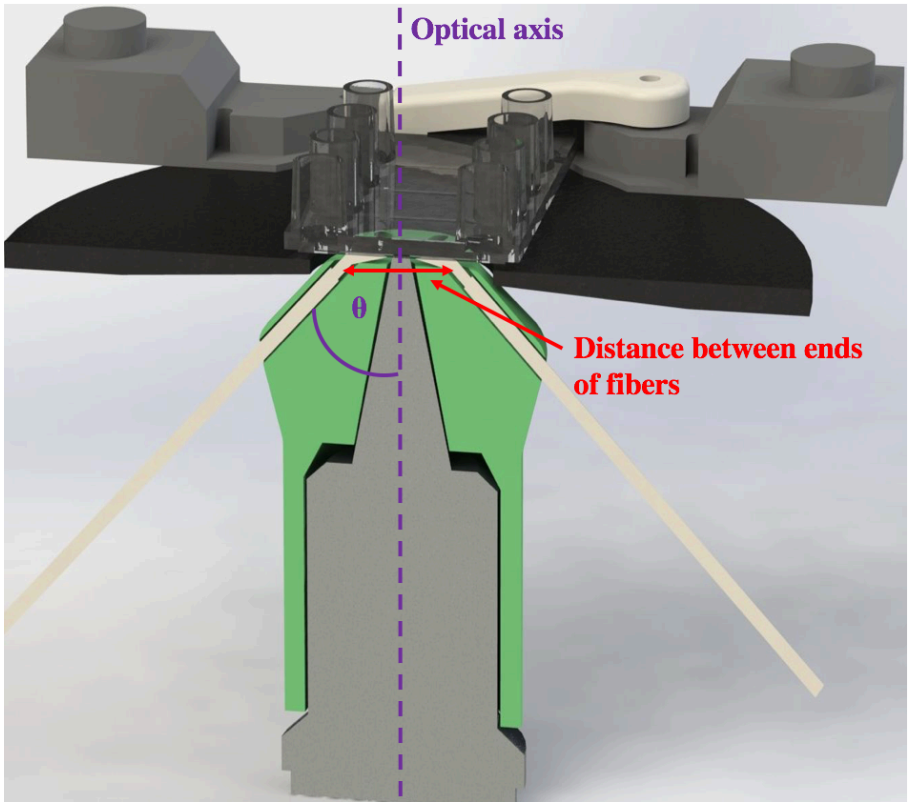

Figure 12. Diagram illustrating two of the experimental variables: fiber incidence angle, θ, and distance between ends of LED fibers.

were used to measure the effects of wavelength on image contrast and SNR. The LEDs were

driven by LED drivers (Thorlabs LEDD1B, T-Cube LED Driver with Trigger Mode, 1200 mA). The sample image was relayed to a complementary metal oxide semiconductor (CMOS) camera (Photon Focus HD1-D1312-160-CL-12).

Several fiber holders were designed and 3D printed to allow variation of fiber incidence angle and the distance between the tips of the fibers (Figure 12, Table 1).

This setup illuminates the bottom of an Ibidi flow chamber, which is placed on the microscope stage (Figure 13). Several different flow chambers were used to vary the depth of the channel and investigate how thickness of the scattering medium impacts image quality (Table 1).

The optical fibers sequentially acquire images, which have similar values for absorption contrast and opposing values of phase contrast. The images can either be added or subtracted in post-processing to maximize either absorption contrast or phase contrast, respectively.

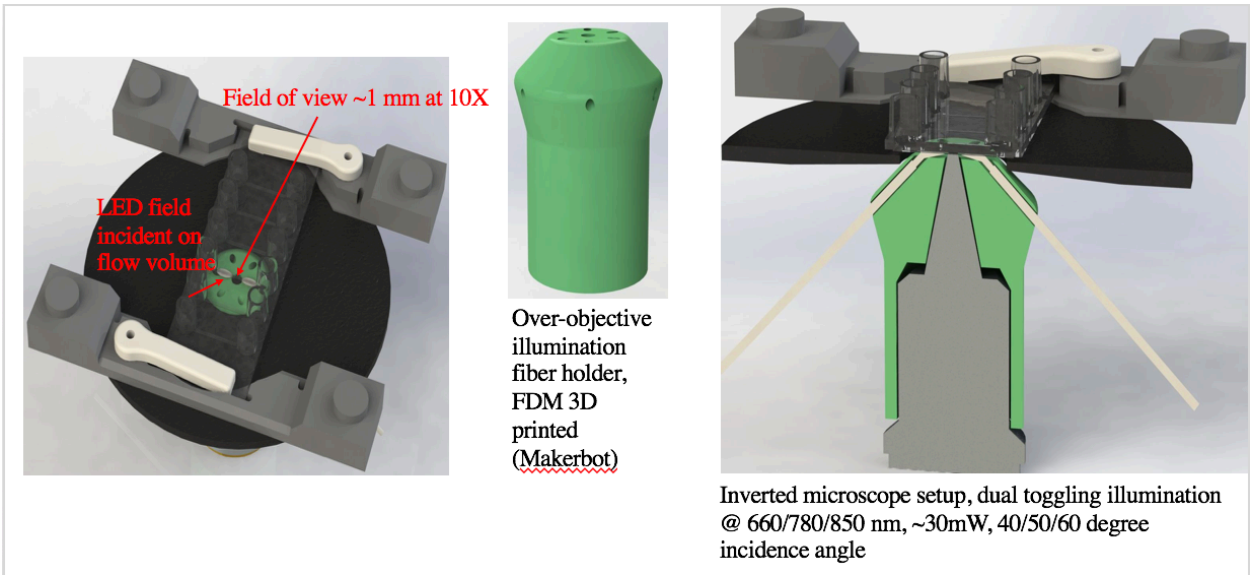

Figure 13. SolidWorks drawings of 3D-printed fiber holders and mounted on 10× objective of Leica microscope and Ibidi flow chamber placed on stage. Field of view is approximately 1 mm at 10× magnification. The LED field is incident on the flow volume. Dual toggling illumination with various LED wavelengths (660 nm, 780 nm, and 850 nm) and incidence angles (40°, 50°, 60°).

2.2.2 Cell Culture

Mouse fibroblast cells (NIH 3T3, ATCC) were grown in tissue culture treated flasks (Corning Life Sciences, T-75 Falcon) with standard cell culture media composed of 90% Dulbecco's Modified Eagle Medium (Sigma-Aldrich), 10% FBS (Sigma-Aldrich), and 1% penicillin-streptomycin (Sigma-Aldrich).

Harvested 3T3 cells were seeded into the ibiTreat flow chambers (Ibidi) with #1.5 polymer coverslip and tissue culture treatment. Flow chambers were mounted on the stage of the inverted microscope along with OBM toggled into the setup (Figure 11).

2.2.3 Whole Blood and Blood Phantom

Fresh venous porcine blood was perfused over the 3T3 cells in flow chambers. 50 mL samples were collected in Luer-lock tip syringes (Covidien 60 mL Monoject^{TM}) coated with lithium heparin (Sigma-Aldrich) following sacrifice of the animal.

Liquid blood phantom were also designed to mimic the optical properties of medium-oxygenated blood for imaging standard. The absorption coefficient, μ_a, was 0.24 mm^{-1} and the scattering coefficient, μ_s, was 1.67 mm^{-1}. India Ink (Beckton, Dickinson and Company) was used as the absorber and Intralipid (Sigma Aldrich) was used as the scatterer. India Ink absorption coefficient was determined using Beer's Law in a simple extinction experiment. Glass beads (Polysciences 07668-1, 10-30 μm diameter) were added to analyze system parameters and optimize setup.

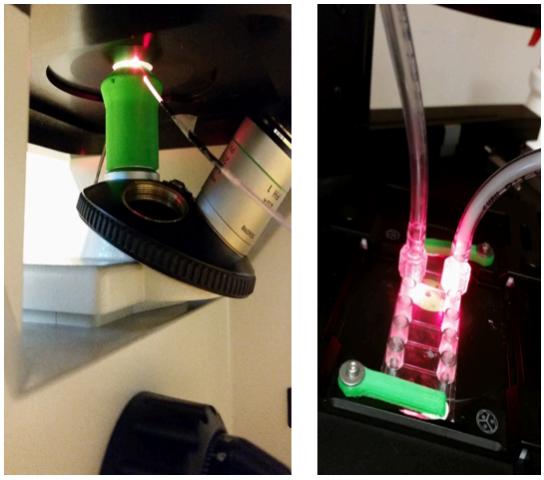

Figure 14. Images showing Ibidi flow chambers fixed on inverted microscope stage while LEDs are illuminating the channel.

Table 1. Experimental parameters that were varied in various permutations to find ideal OBM settings to achieve optimal image quality.

LED wavelength	Fiber Angle	Distance between Fibers	Depth of Flow Chamber
660 nm	40º	6 mm	100 μm
770 nm	50º	8 mm	200 μm
850 nm	60º	10 mm	400 μm
	70º	12 mm	600 μm
			800 μm

2.2.4 Regulation of Blood Flow and Perfusion Pumps

When monolayers were confluent, flow chambers were perfused with whole blood or blood phantom at 5 dynes/cm^2 using a programmable syringe pump (Braintree Scientific BS-8000, 120V). The system operates by passing perfusate between two pump-mounted syringes that push and pull in alternating directions.

Assuming a parabolic flow pattern, the shear stress, τ, of flowing blood in an Ibidi chamber is related to the viscosity of the perfusate, the flow rate, and a constant factor by a set of relationships provided by the manufacturer (ibidi GmbH, 2016). The flow rates for each type of flow chamber to obtain a shear stress of 5 dynes/cm^2 (which most closely replicates the

conditions of the Bioflux system) were calculated in Table 2. The viscosity of blood was assumed to be 0.032 dynes·s/cm^2 (Litwin & Chapman, 1970).

Table 2. Flow rates for various Ibidi flow chambers that to achieve shear stress of 5 dynes/cm^2. τ is shear stress, η is the viscosity of blood and Φ is the flow rate (ibidi GmbH, 2016).

Ibidi Flow Chamber	**Channel Depth**	**Shear Stress Equations (μl / min)**	**Flow Rate (corresponding to shear stress of 5 dynes/cm^2)**
μ-Slide I$^{0.8}$ Luer	800 μm	$\tau = \eta \cdot 34.7 \cdot \Phi$	4.5 mL/min
μ-Slide I$^{0.6}$ Luer	600 μm	$\tau = \eta \cdot 60.1 \cdot \Phi$	2.6 mL/min
μ-Slide I$^{0.4}$ Luer	400 μm	$\tau = \eta \cdot 131.6 \cdot \Phi$	1.2 mL/min
μ-Slide VI$^{0.4}$	400 μm	$\tau = \eta \cdot 176.1 \cdot \Phi$	0.89 mL/min
μ-Slide I$^{0.2}$ Luer	200 μm	$\tau = \eta \cdot 512.9 \cdot \Phi$	0.30 mL/min
μ-Slide VI$^{0.1}$	100 μm	$\tau = \eta \cdot 10.7 \cdot \Phi$	14.6 μL/min

2.2.5 Experimental Design

Several sets of experiments were carried out to demonstrate the performance of OBM compared with PC under increasingly difficult conditions. First, objects with known and strong phase contrast (glass beads) were imaged with in a blood phantom of known optical properties. Second, glass beads were imaged in whole blood. Third, 3T3 cells were imaged in whole blood. Paired OBM and PC images were acquired in all experiments, and the experimental parameters of the setup (Table 1) were varied in different combinations, along with the exposure time, digital gain, and frame rate of the camera.

2.3 Results

2.3.1 Beads in Blood Phantom

Proof of principle was first demonstrated by imaging glass beads in a controlled and well-characterized scattering environment. The first channels to be imaged were the 400 μm deep

channels. The thickness of these channels makes them most likely to have least phase contrast in Zernike. The Zernike video in Figure 15A shows worse contrast than the OBM image in Figure 15B. Given the depth of the channel, it was likely that the absorbing agent (India Ink) had absorbed a significant part of the signal. As seen in the Z-stacks (Figure 16), the beads never came into focus with Zernike but they were seen sharply focused with OBM. Phase artifacts in deep specimens and halo effects tended to distort Zernike images, so the perimeter of the beads did not have clearly defined borders, but instead appeared blurred.

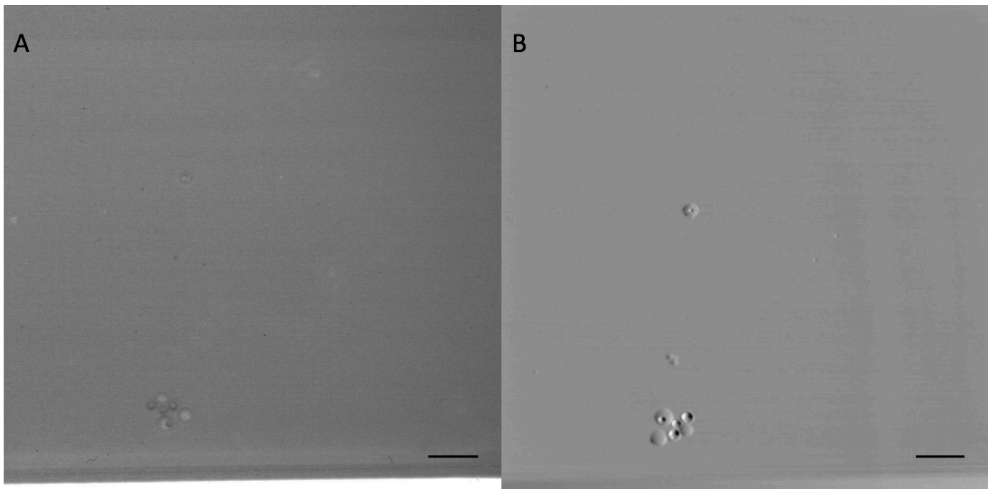

Figure 15. (a) Zernike phase gradient images and (b) OBM images of 10-30 μm glass beads under blood phantom flow at 5 dynes/cm^2 in 400 μm depth Ibidi flow chamber. Scale bar 100 μm. See Supplement for video.

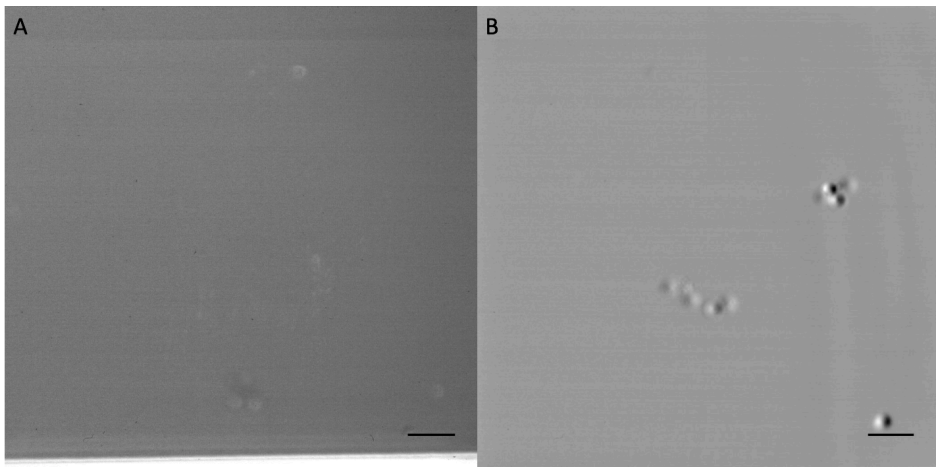

Figure 16. Z-stacks focusing through each plane of (a) Zernike phase gradient images and (b) OBM images of 10-30 μm glass beads under blood phantom flow at 5 dynes/cm^2 in 400 μm depth Ibidi flow chamber. Scale bar 100 μm. See Supplement for video.

In thinner channels of 100 μm depth, the image quality of Zernike image improved while the image quality of OBM was not significantly altered (Figure 17, Figure 18). Zernike produced the highest quality images in thin channels, while OBM imaging was optimal in thick channels. The halo effect was significantly more pronounced in the Zernike images in Figure 17 and Figure 18 compared to those in Figure 15 and Figure 16.

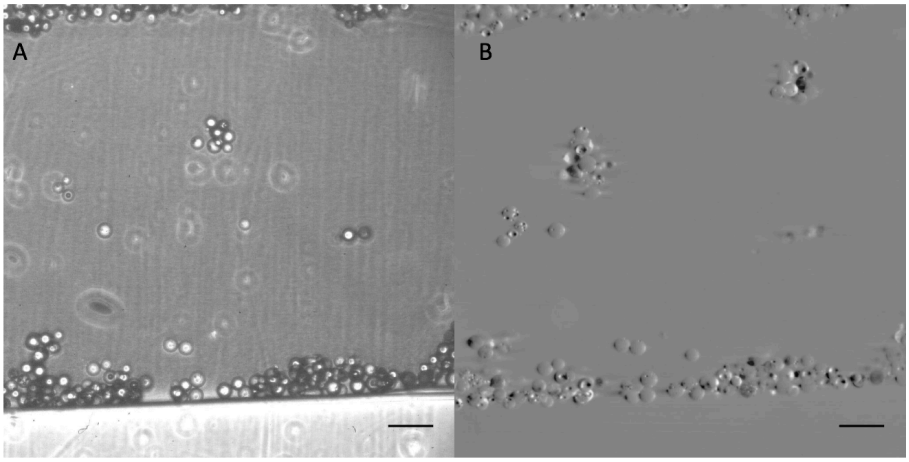

Figure 17. (a) Zernike phase gradient images and (b) OBM images of 10-30 μm glass beads under blood phantom flow at 5 dynes/cm^2 in 100 μm depth Ibidi flow chamber. Scale bar 100 μm.

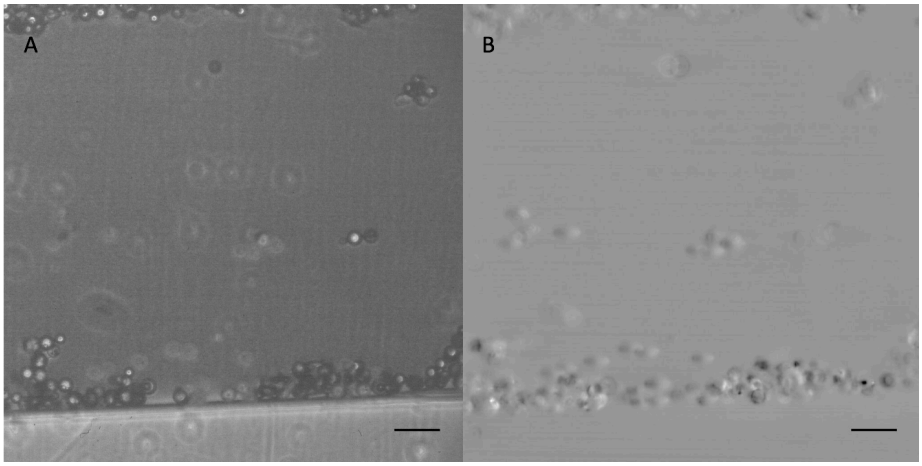

Figure 18. Z-stacks focusing through each plane of (a) Zernike phase gradient images and (b) OBM images of 10-30 μm glass beads under blood phantom flow at 5 dynes/cm^2 in 100 μm depth Ibidi flow chamber. Scale bar 100 μm

2.3.2 Glass Beads in Whole Blood

Imaging of glass beads in whole blood illustrated that OBM captures higher quality images than Zernike. However, Zernike contrast is improved in the thinner channel (Figure 15A, Figure 16A) because Zernike phase contrast is weakened when there is a highly scattering background present. OBM phase contrast is not significantly different between channel depths (Figure 19B, Figure 20B).

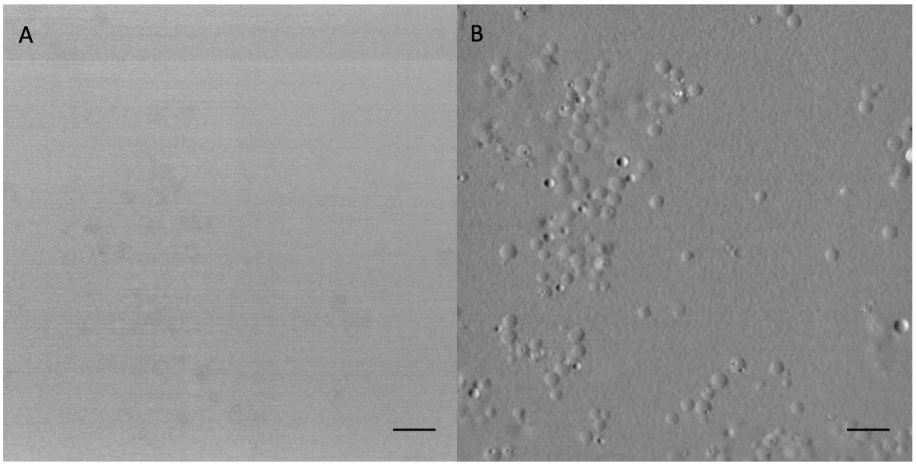

Figure 19. (a) Zernike phase gradient images and (b) OBM images of 10-30 μm glass beads under whole blood flow at 5 dynes/cm^2 in 400 μm depth Ibidi flow chamber. Scale bar 100 μm. See Supplement for video.

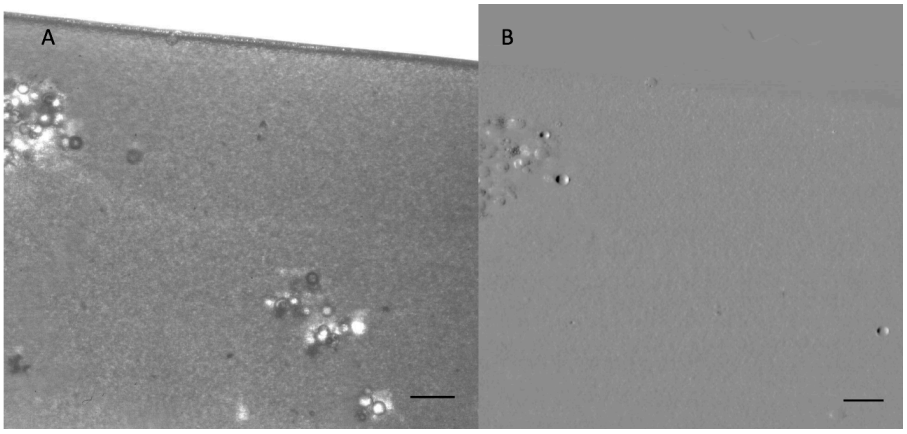

Figure 20. (a) Zernike phase gradient images and (b) OBM images of 10-30 μm glass beads under whole blood flow at 5 dynes/cm^2 in 100 μm depth Ibidi flow chamber. Scale bar 100 μm. See Supplement for video.

2.3.3 3T3 Cells in Whole Blood

The first images acquired of the 200 μm channels with OBM showed significantly more morphological detail of the 3T3 monolayer than the images acquired with Zernike (Figure 21). The outlines of the cells are well-defined (Figure 21B) and align well with the image taken before blood was perfused through the channel (Figure 21A). As the depth of the channel decreased to 100 μm, the quality of Zernike images improved slightly (Figure 22B).

Figure 22 shows in 100 μm, the cells are not well defined with Zernike. The general texture of cells is apparent, but not with definition. However, OBM demonstrates clear definition of the monolayer, as well as neutrophils that have adhered to the bottom of the plate. Identification of neutrophils made based on their size relative to the 3T3 cells and their adhesive behavior, which is characteristic of neutrophils.

Further, OBM displayed subcellular features of 3T3 cells (Figure 23). Nucleoli of cells are visible for nearly all cells. Lastly, Figure 24 video shows a neutrophil approach a 3T3 cell, adhere to it for a brief interaction, and then flow away.

Table 3 shows the optimal optical parameters that were identified for producing high-quality images with 100 μm channels. Despite the attempt to find a single set of optimal optical parameters, it was found that there is rather an optimal range of parameters that reflects the optimal geometrical setup.

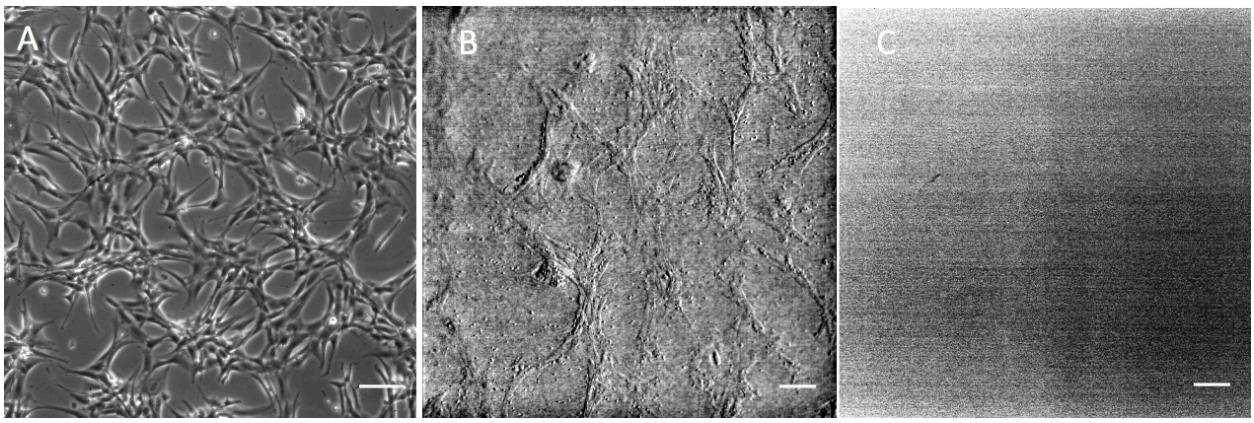

Figure 21. Comparison of Zernike and OBM imaging of 200 μm depth Ibidi channels with 5 dynes/cm^2 shear rate. (a) 3T3 monolayer imaged through cell culture medium. (b) OBM image of 3T3 monolayer through whole blood. 100 ms exposure, 50º incidence angle, 660 nm LED wavelength, 12 mm distance between fiber ends, 1× digital gain. (c) Comparable Zernike image of 3T3 through whole blood. Scale bar 100 μm.

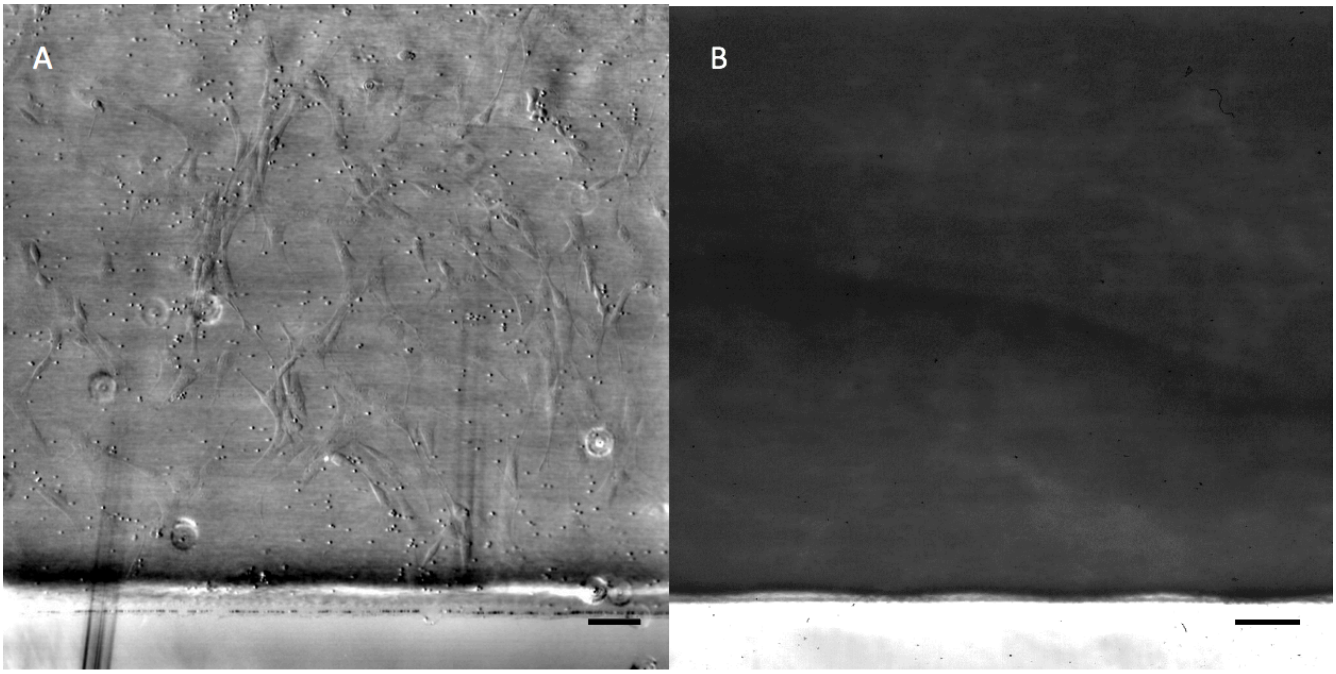

Figure 22. Comparison of OBM and Zernike imaging of 100 μm depth Ibidi channels with 5 dynes/cm^2 shear rate. (a) OBM image of 3T3 monolayer through whole blood. 70 ms exposure, 60º incidence angle, 660 nm LED wavelength, 8 mm fiber separation, 1× digital gain. (b) Comparable Zernike image of 3T3 with identical settings through whole blood. Scale bar 100 μm.

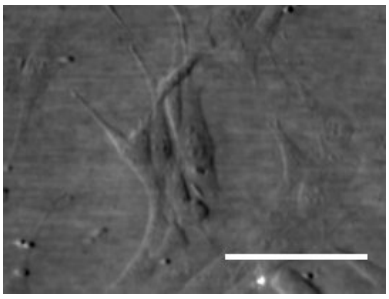

Figure 23. OBM image of 3T3 cells under whole blood flow in 100 μm depth Ibidi channel. Sub-cellular features, notably nucleoli are visible. 90 ms exposure, 60º incidence angle, 660 nm LED wavelength, 12 mm fiber separation, 1× digital gain. Scale bar 100 μm.

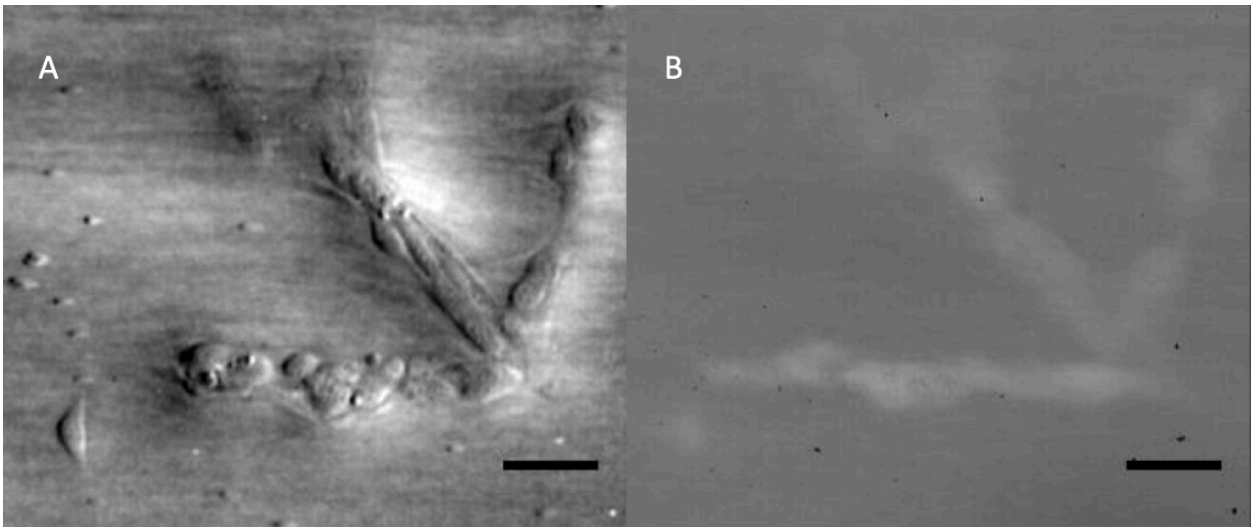

Figure 24. Comparison of OBM and widefield imaging of 100 μm depth Ibidi channels. (a) OBM shows neutrophils as they approach endothelium, interact with surface, before flowing away. 100 ms exposure, 60º incidence angle, 660 nm LED wavelength, 8 mm fiber separation, 1× digital gain. (b) Comparable widefield image of same area under same conditions. Scale bar 50 μm. See supplement to watch video.

Table 3. Optimal optical parameters for OBM imaging in Ibidi flow chambers

Parameter	**Optimal Setting**
LED wavelength	660 nm
Distance between LEDs	8 – 12 mm
Incidence Angle	60°

2.4 Discussion

In experiments using deepest channels (800 μm, 600 μm, 400 μm), no clear images were produced. Once cell culture techniques were optimized, depths of the channels were decreased and ideal optical parameters of OBM were found, better OBM images were obtained of 3T3 cells under whole blood perfusion.

OBM has been demonstrated to be suitable for imaging endothelial cells under a flow of blood in a commercial flow chamber. OBM was sensitive to the specular reflections from the boundaries of the flow chamber. The system-specific geometric patterns (fiber incidence angle, fiber separation, LED wavelength) that govern specular reflections and other sources of background were determined and used to guide the optimized design of the fiber holder for the BioFlux system (Table 3). Rather than finding a single optimal configuration of optical parameters to improve image quality, a general range of parameters with similar geometric properties were determined. Optimal OBM image contrast and SNR were products of a general geometric configuration versus a specific wavelength, fiber incidence angle, and fiber separation (Table 3).

Figure 15 - Figure 20 demonstrated that the phase contrast of glass beads in solution were stronger when beads were imaged with OBM rather than Zernike. This suggested that at depths greater than tens of micrometers, the Zernike signals fell off because the image of the annular illumination becomes misaligned with the phase ring if multiple scattering occurs in the beam path. The beads also appeared distorted when imaged with Zernike due to phase artifacts and the halo effect, which blurred the perimeter of the beads. Once the depth of the channel was 400 μm, there was effectively no reference field, so phase sensitivity was lost, and the Zernike image quality was as good as a widefield image. The second reason that Zernike images were poorer

quality than OBM images is due to absorptive contrast. The illumination could not penetrate through the thick, scattering medium, so the SNR decreases because insufficient photons were collected. The data agree with these hypotheses regarding the disadvantages of Zernike microscopy.

When compared with Zernike phase contrast images, it was evident that regardless of the depth of the scattering medium, OBM provided better image contrast than Zernike imaging of 3T3 cells (Figure 22). As predicted, Zernike cannot image through more than tens of micrometers of whole blood due to high optical scattering and absorption. Furthermore, OBM provided sub-cellular resolution of nucleoli within the 3T3 cells, which was could not be viewed when imaging the cells through growth medium with phase contrast microscopy (Figure 23). The high-resolution of OBM, interactions between the endothelium and neutrophils in the perfusate could be observed (Figure 24). Neutrophils approached the endothelium, and slowed down upon docking on individual cells, so their signal could not be detected, and as they flowed away their zero-mean signal was averaged. This capability has promising utility for improving understanding of the interaction between ECs and immune modulators in the blood.

OBM could only be performed when blood was flowing because endothelial cell contrast was obscured by red blood cell and neutrophil contrast when they were both in same the focal plane. In future assays it will be important to average the zero-mean neutrophil signal. This will be more accurate because relevant physiological assays are performed under flow conditions. Strong signals from RBCs obscure relatively weaker signals from ECs. Because a property of OBM is that the contrast is zero-mean, especially for spherical objects, we can reduce the contrast from the RBCs by flowing them during an exposure time. This blurs out the RBC background signal reducing it to its average value of zero.

2.5 Conclusion

OBM has been demonstrated to image through thin scattering medium. OBM image quality was found to be higher than Zernike images. Phase contrast was stronger when imaging with OBM and the borders of 3T3 cells were more well-defined. Additionally, OBM images of 3T3 cells display subcellular features of cells, which were not visible with Zernike. No single optimal combination of optical parameters, but rather a range of parameters allowing for highest quality images, was observed (Table 3). The optimal wavelength was 660nm, the best incidence angle was 60 degrees, and the range of distances between optical fibers was 8 – 12mm. Based on the general principle of the fiber holder designed for this experiment, the holder was redesigned and appropriated for the Bioflux system.

An important future direction is to identify exactly what are the adherent cells that we have suggested were neutrophils. Due to their size ratio compared to the ECs and their characteristic property of adhering to the bottom of the channel, they were suggested to be neutrophils, but further studies to confirm this identification, perhaps via fluorescence tagging, would be necessary.

Chapter 3 OBM Setup for BioFlux Imaging Platform

3.1 Introduction

The Pierson lab at the University of Maryland Medical Center is a transplant immunology group that strives to understand how the immune system works in the context of transplantation to enable transplant between species. Their group is specifically interested in finding an imaging technique that is compatible with their Bioflux platform to image porcine aortic endothelial cells (PAOECs) under whole blood flow to monitor the host versus graft cellular interactions. Upon successfully designing a setup of OBM that would be compatible with the Ibidi system, the setup was modified for the Bioflux system. Once the components were designed and manufactured at MGH, the parts were shipped to the Pierson lab at the University of Maryland Medical Center and all further experiments were performed on the campus in Baltimore, MD.

3.2 Methods

3.2.1 BioFlux Setup

The BioFlux 1000Z system is a fully-integrated system capable of performing high-throughput shear flow assays (Figure 25). The microscope used in the system is a Zeiss Z1 Axio Observer inverted microscope, which includes a 10× objective (Zeiss A-Plan 10×/0.25 Ph1). The system also includes the BioFlux controller, which is a pneumatic pressure controller and a perfusion pump, a well plate interface, automated stage, and high-resolution camera (Photometrics CoolSNAP HQ2 CCD Camera). There is a double adapter (Zeiss Double Adapter DuoLink) which can mount two camera ports. The adapter includes a slider with a 100% mirror

to toggle between cameras. The two cameras mounted in the adapter were the CoolSNAP (for PC imaging) and Photon Focus HD1 (for OBM imaging).

Once cells have been cultured and pipetted into the individual channels, the plate is mounted onto a heating plate which contains holes to allow for imaging of the channels while the plate is heated at physiological temperature 37 ºC. The heating plate is then fitted into the automated stage and the flow inlets are attached to the plate. The perfusate is not recirculated.

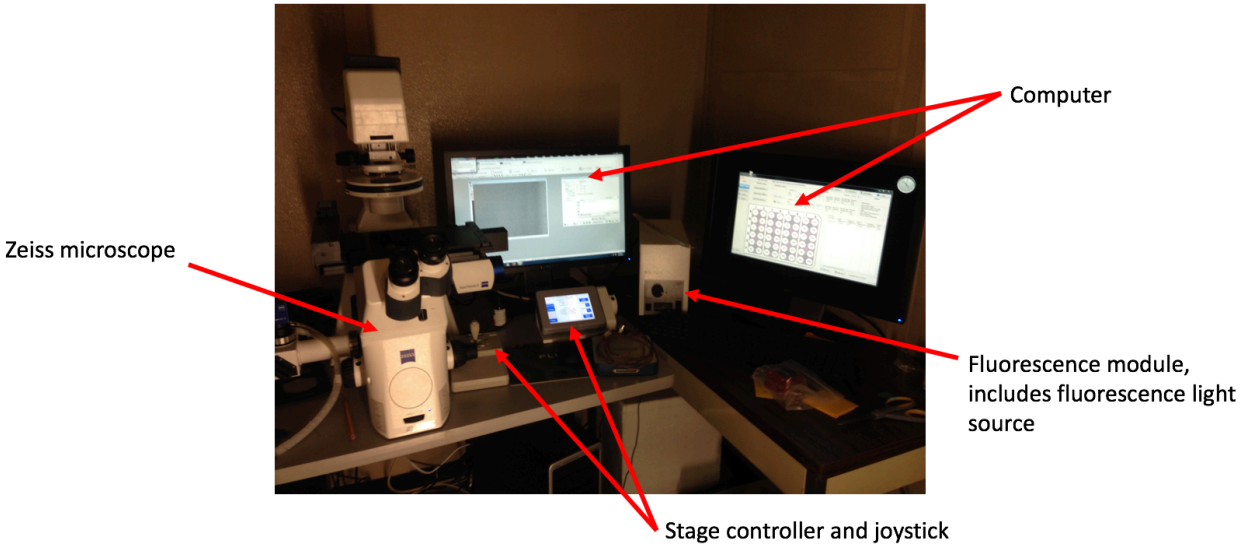

Figure 25. Bioflux 1000Z setup is a fully-integrated *in vitro* live cell assay imaging platform. The setup includes a Zeiss Z1 Axio Observer inverted microscopy, a pneumatic pump (not displayed), a computer, and fluorescence module.

3.2.2 Flow Chambers

Before cell seeding, the channels in the BioFlux plate were coated with 100 μg/mL bovine plasma fibronectin (Sigma-Aldrich) in phosphate buffered solution (PBS) via perfusion for 5 minutes at 5 dynes/cm^2 (shear rate 125/s). The fibronectin was allowed to settle for 1 hour at room temperature 23 ºC. Following this, the channels were washed with culture media composed of DMEM, FBS, gentamicin, and amphotericin B at 5 dynes/cm^2 for 10 minutes. 40 μL of cell suspension was seeded into the inflow wells.

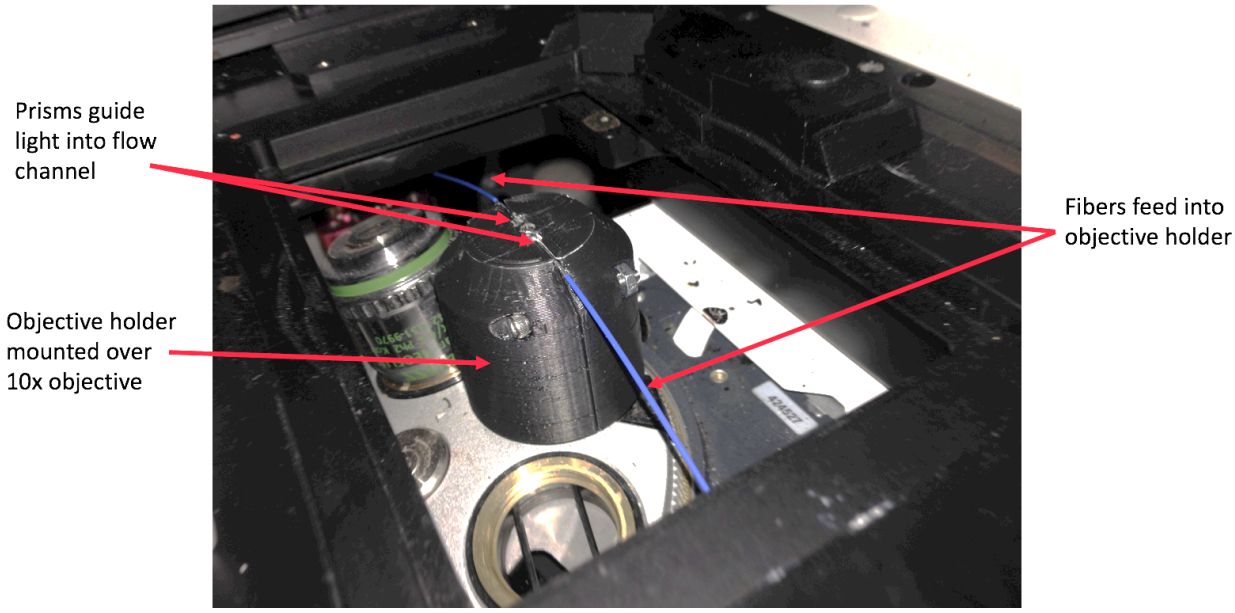

Figure 26. Fiber holder is mounted onto Zeiss 10× objective, and then optical fibers are guided into the holder. At the ends of the fibers, prisms guide the illumination into the channel.

3.2.3 Cell Culture

Porcine thoracic aortae were excised after heart-lung explantation and used to culture primary aortic endothelial cells (PAOECs). By scrapping the aortae, GalTKO.hCD46 and GalTKO.hCD46.hEPCR PAOECs were isolated and seeded in tissue culture treated flasks coated with 0.5% gelatin (Sigma-Aldrich). The cells were grown in standard cell culture medium, which was composed of 90% DMEM with 1 g/L D-glucose, 110 mg/L sodium pyruvate and L-glutamine (Gibco-Life Technologies), 10% FBS (Atlanta Biological), gentamicin, and amphotericin B. An endothelial cell growth supplement was added at 100 μg/mL for the first passage of the PAOECs and 50 μg/mL were used for subsequent passages. The cells were passaged every three days. Cells were only used for experimentation between the 4th and 8th passages. Cells were harvested via trypsinization with 0.25% trypsin (Gibco) and suspended at a density of 10×10^{6} cells/mL of cell culture medium. The T-75 flasks were incubated at 37 ºC and 5% CO_2.

3.2.4 Whole Blood

Fresh human whole blood was collected in 4-8 mL samples via venipuncture using sodium heparin coated vacutainers (Becton Dickinson, 75 units/4 mL).

3.2.5 Perfusions

Two different perfusion experiments were performed. Each experiment varied either the perfusate, which had different optical characteristics of the scattering medium to investigate how OBM behaves under various conditions.

3.2.5.1 Whole blood flowing over PAOECs

350 μL of whole blood perfusate was pipetted into the inflow wells of the experimental channels. In order to simulate physiologic flow, such as that found in the microcirculation of pulmonary vasculature, the blood was perfused at 5 dynes/cm^2 and 37 ºC for 50 minutes.

Two types of whole blood were perfused over the monolayer: both high (10 u/mL) and low (3 u/mL) heparin concentration, in order to investigate how OBM is affected by the speed and relative extent of thrombus formation in the channel.

Both PC and OBM images were acquired once every minute over the course of the assay.

3.2.5.2 Diluted blood flowing over PAOECs

Diluted blood was composed of isolated RBCs and neutrophils. Three concentrations (weight/volume) of diluted blood were used as perfusate: 0% RBCs and 100% neutrophils; 25% RBCs and 75% neutrophils; 50% RBCs and 50% neutrophils; 75% RBCs and 25% neutrophils. RBCs were separated from human whole blood via buffy coat separation and neutrophils were separated from whole blood via standard density gradient separation.

3.2.6 Phase Contrast Imaging

Phase contrast images were acquired at 10× magnification with a 100 ms exposure every minute over the course of each experiment.

3.2.7 OBM Fiber Holder

A fiber holder was designed and manufactured for the specific dimensions of the Zeiss Z1 Axio Observer microscope that is part of the BioFlux system at the Pierson lab at the University of Maryland Medical Center (BioFlux 1000Z, Fluxion Biosciences) (

Figure 27). The holder was designed so that the endothelial cell monolayer would be in focus while accounting for the working distance of the 10× objective (4.5 mm) and the distance between the top of the objective and the bottom of the monolayer in the BioFlux plate (

Figure 27).

The configuration of the BioFlux system posed significant geometrical constraints that prevented a simple redesigning of the former fiber holder design (simply changing the dimensions of the inner chamber to fit the Zeiss 10× objective), so a new concept was conceived that incorporated two prisms attached to the ends of each LED-coupled fiber to guide the illumination into the flow chamber (Figure 28). The former 60º incidence angle was no longer feasible because the objective itself is wider and the imaging area, which is controlled by the size of the holes in the heating plate.

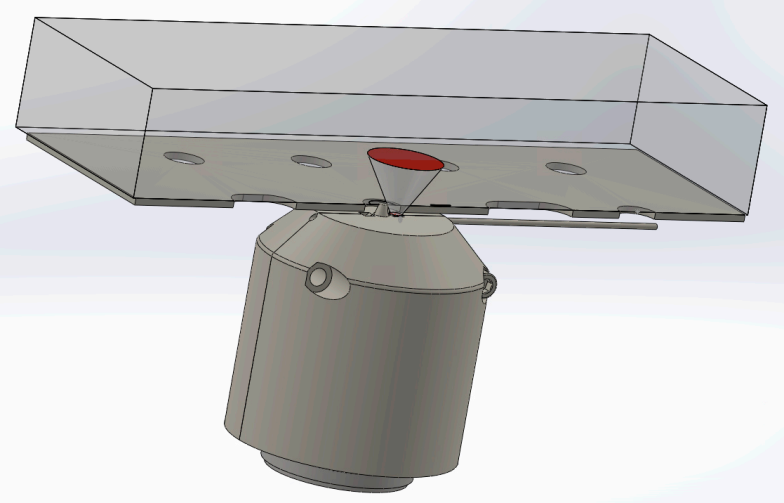

Figure 27. 3D-printed fiber holder designed and manufactured for Bioflux system. Conditions of the setup were simulated in SolidWorks to properly model the system and design the holder.

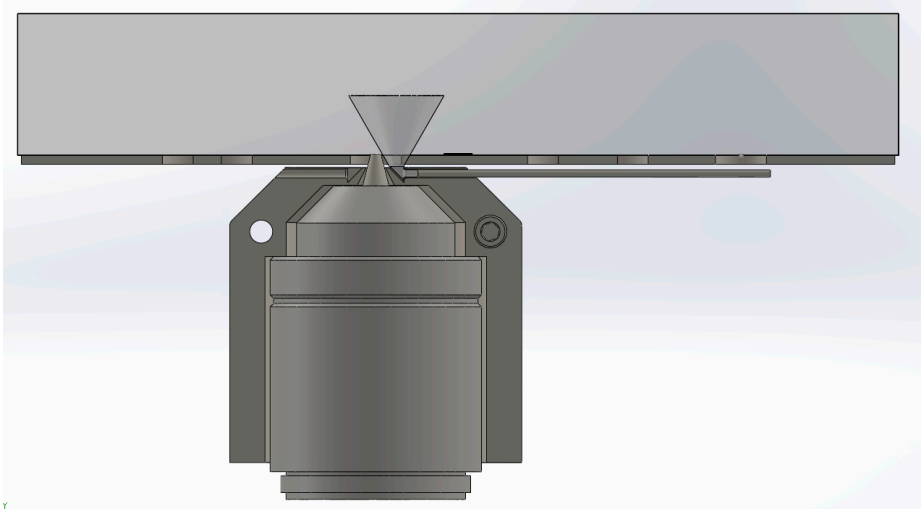

Figure 28. Side-view of 3D-printed fiber holder.

3.2.8 OBM Imaging

OBM images were acquired once every minute over the duration of each experiment. The exposure time, net frame rate, and digital gain were adjusted throughout the experiment to optimize image contrast, SNR, and visibility of the monolayer.

3.2.9 Image Processing

The images were processed manually in ImageJ (U. S. National Institutes of Health, Bethesda, MD) by first isolating the region of interest, the channel, from each raw image. The

cropped left and right raw image stacks (from the left and right LEDs) were divided by their temporal average, thus image intensity represented percent deviation from the average intensity. These left and right images were then subtracted from one another to enhance phase gradient contrast. The final image contrast was then manually adjusted so that the pixel value range would be symmetric around zero and the middle gray represented the background.

3.3 Results

OBM was demonstrated to provide images of the monolayer with weak contrast, but imaged neutrophil adhesion to the plate with stronger contrast. When imaging PAOECs under whole blood flow, the endothelium was hardly visible, although the general texture of the monolayer was observed (Figure 29). Contrast of neutrophils was improved (Figure 29B) over phase contrast images acquired with Bioflux Zeiss microscope (Figure 29A).

Interestingly, as large thrombus perfused over monolayer (likely due to buildup upstream in the channel), monolayer becomes visible in the area under the thrombus. In other parts of the channel, the monolayer is not as distinctly visible (Figure 30).

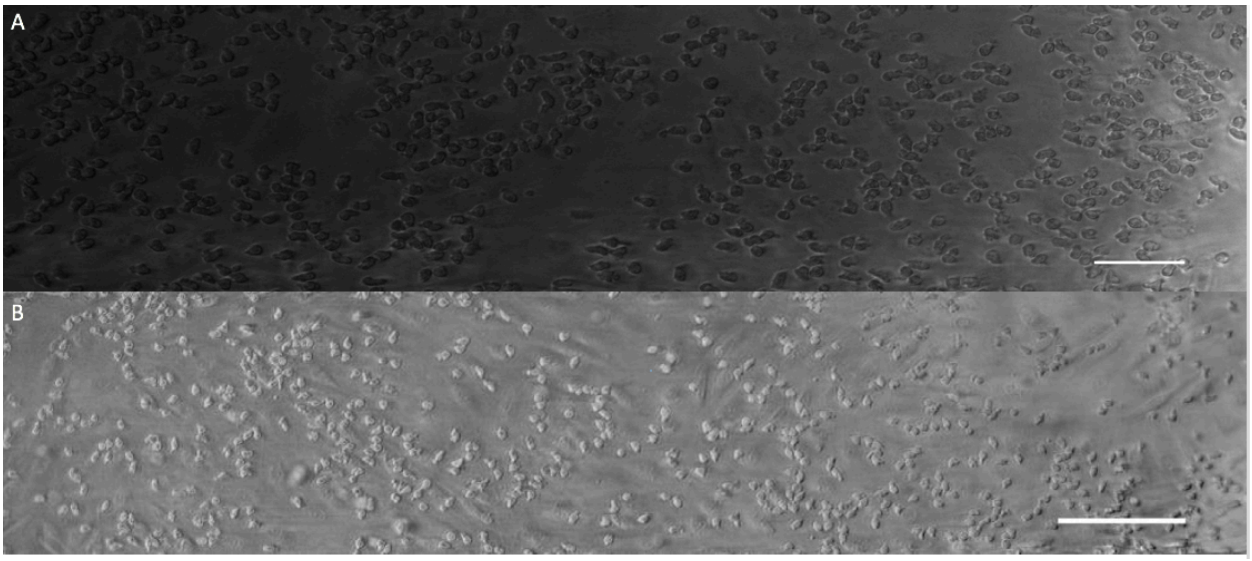

Figure 29. (a) Phase contrast and (b) OBM image of PAOECs with whole blood flow in 70 μm deep channels. 100 ms exposure, 2.4 Hz frame rate, 1× digital gain. Time-averaged image. Neutrophils adhere to monolayer. Scale bar 100 μm.

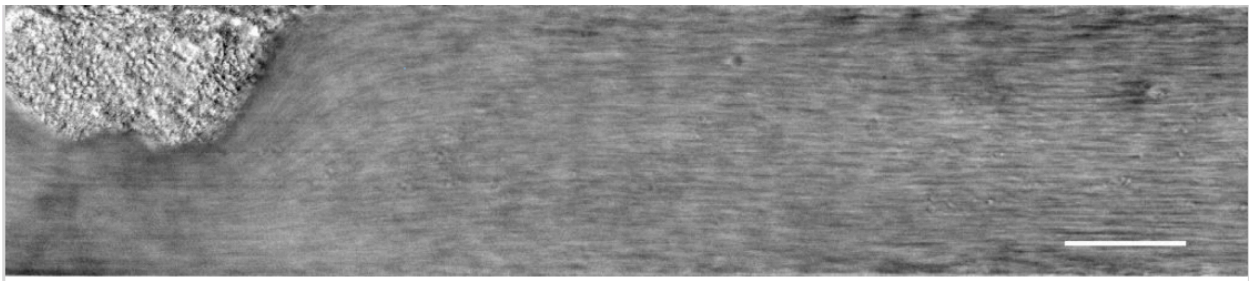
Figure 30. Thrombus flowing through Bioflux channel with PAOECs and whole blood perfusate. Areas of monolayer becomes visible as thrombus passes over them. 100 ms exposure, 2.4 Hz frame rate, 1× digital gain. Scale bar 100 μm. See supplement to watch video.

In perfusion experiments with diluted concentrations of blood, the monolayer was most visible when there were no RBCs in perfusate (Figure 31). In all concentrations of diluted blood, however, the neutrophils which adhered to the bottom of the channel had relatively similar phase contrast. The monolayer was least visible when the diluted blood solution was composed of 50% RBCs (Figure 33).

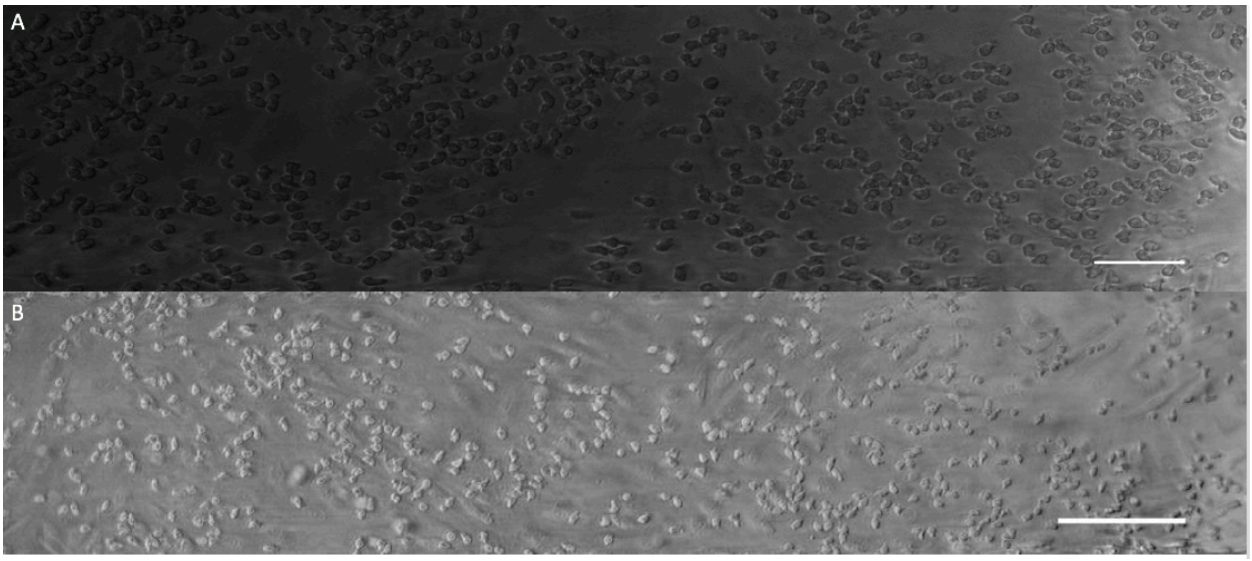

Figure 31. OBM image of perfusion of 75% neutrophil and 25% RBCs solution over monolayer. Neutrophils adhere to monolayer and roll. 660 nm LEDs, 100 ms exposure, 2.4 Hz frame rate. Scale bar 100 μm. See supplement to watch video.

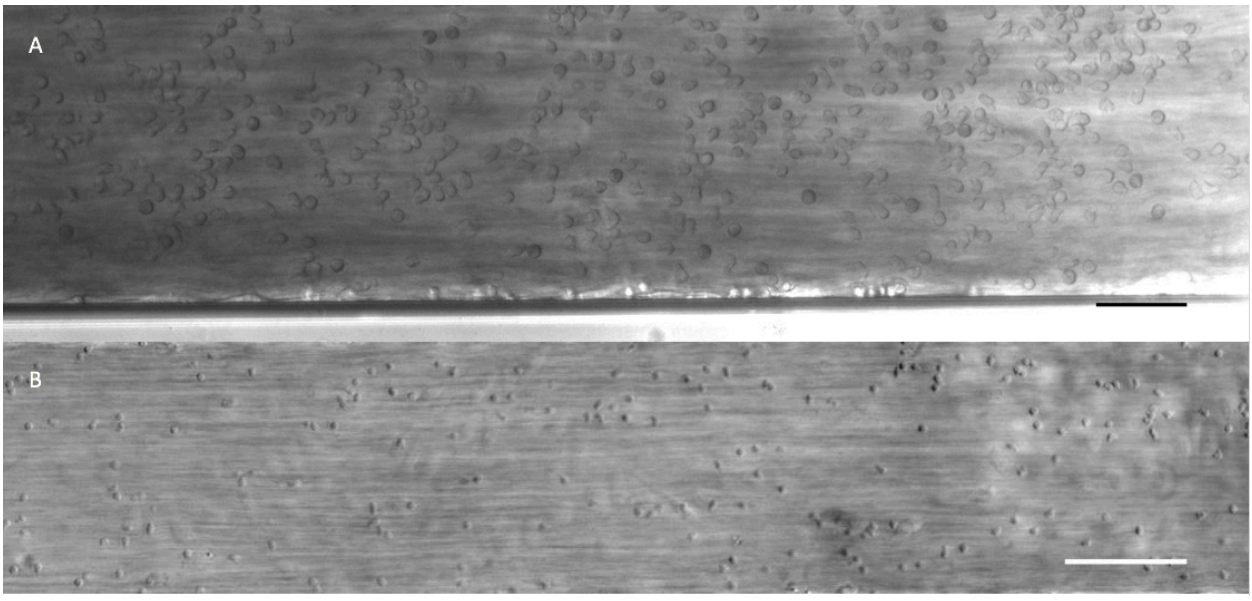

Figure 32. OBM image of perfusion of 75% neutrophil and 25% RBCs solution over monolayer. Neutrophils adhere to monolayer and roll. 660 nm LEDs, 100 ms exposure, 2.4 Hz frame rate. Scale bar 100 μm. See supplement to watch video.

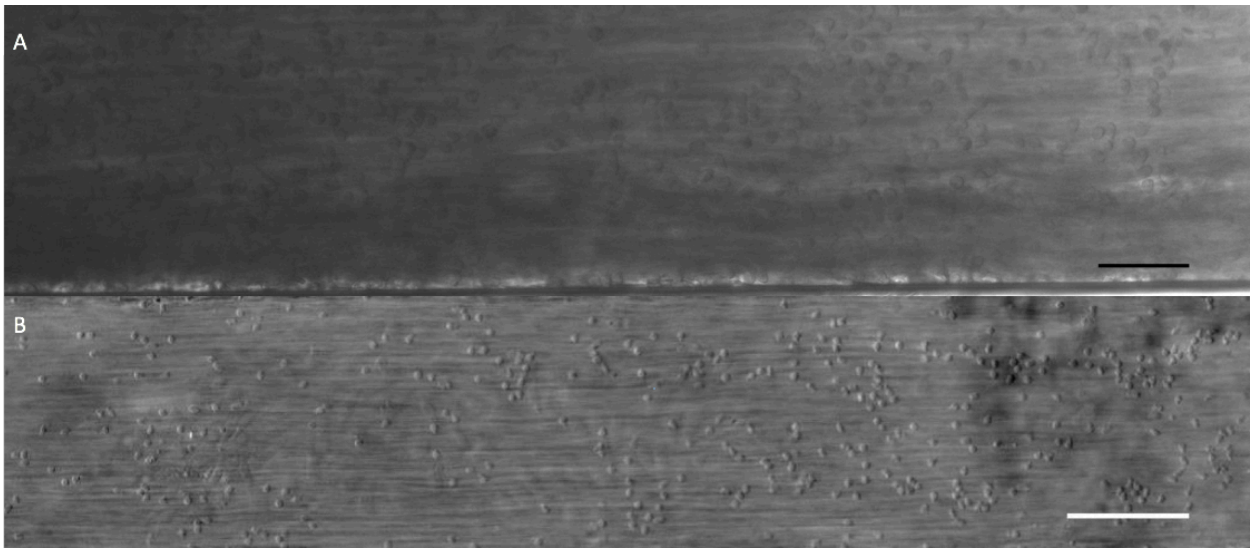

Figure 33. (a) Phase contrast and (b) OBM image of perfusion of 50% neutrophil and 50% RBCs solution over monolayer. Neutrophils adhere to monolayer and roll. 660 nm LEDs, 100 ms exposure, 2.4 Hz frame rate. Scale bar 100 μm. See supplement to watch video.

3.4 Discussion

This work demonstrated that PAOECs and neutrophils could be viewed minimally using various blood flow conditions. The texture of cells was visible but not with high definition. It is possible that the new concept of attaching prisms to the ends of the optical fibers resulted in too much light lost on the opposite side of the channel. As a result, fewer photons were collected at the detector with the result being poorer contrast than that obtained in the previous setup for the Ibidi system.

Another potential area of difficulty was that the thinner optical fibers had less throughput, so fewer photons would have been delivered to the sample leading to decreased contrast of the endothelium. Decreasing the inner diameter by half requires a four-fold increase in exposure time to theoretically obtain the same result. Since a longer exposure time builds dark noise background bias, the increase of exposure time length had to be balanced with the buildup of background.

One problem with the design that was encountered in experiments performed in Maryland was that the heating plate was thicker than the working distance of the objective after fiber-holder modification, which prevented the ECs from achieving best focus. Thus, imaging had to be conducted with the non-heating plate insert into the stage. It is important when redesigning the fiber holder to ensure that the thickness of the top of the holder is decreased so that the monolayer can be focused when using the heating plate in place to most accurately recapitulate physiological conditions. Given the short working distance of the Zeiss 10× objective (4.5 mm) rather than the longer working distance of the Leica 10× objective (17 mm), it was harder to create sufficient space between the top of the fiber holder and the monolayer in the Bioflux plates. A wavelength of 660 nm was deemed the optimal wavelength regardless of the types of perfusate used because it delivers the most power to the sample, and in all cases, the short wavelength illumination led to brighter images. When imaging diluted blood (combination of RBCs and isolated neutrophils), it was observed that the signal gradually dropped off as RBC concentration increased.

The fiber holder design including prisms posed difficulty because the prisms could not be securely adhered to the ends of the fibers without risk of the fibers falling off. This design would be more complicated to implement commercially, so it is preferable to optimize the fiber holder design so that the fibers can be inserted into the holder without the prisms.

3.5 Conclusion

The future directions of this work include a redesign of the fiber holders without prisms, so that they adopt a closer resemblance of the fiber holders in Chapter 2. It is likely that with the illumination being perpendicular to the sample, too much optical power was lost over the channel. This is because the channel was exceptionally thin, and so the light was poorly coupled

into the channel to reach the detector. Without the high extent of multiple scattering in the sample, insufficient photons were collected and a proper image could be formed with strong phase contrast. Previously, orthogonal illumination worked when OBM was first implemented in endomicroscopy (Ford, Chu, & Mertz, 2012) because the tissue was so thick, so the angle of illumination did not matter because the tissue was so thick that the photons would eventually be scattered by a layer of the sample and could be collected by the detector.

Another important direction would be to automate the acquisition of OBM images. In order to capture images at even intervals during an assay, the system must be automated similar to the Bioflux system. Ideally, the software for OBM image collection would be integrated into the existing Bioflux image acquisition software.

After creating an optimal setup for the Bioflux system, it would be important to explore various paradigms in biomedical research, ex. thrombosis, leukocyte homing studies (rolling, adhesion, transmigration), endothelial dysfunction, tumor metastasis through circulatory system, and stem cell differentiation.

Lastly, an interesting direction to translate this technology would be to create an *in vivo* OBM probe that could monitor endothelial cells in the vasculature of humans after they have received a xenotransplant. Implementing OBM would be advantageous in that it could be operated in a reflection geometry, like other optical imaging techniques that have been previously translated to *in vivo* probes. This probe could be designed and manufactured for clinical applications after it has been fully characterized and studied for *in vitro* applications.

Abbreviations

CCD: Charge-coupled device

CD46: Complement regulatory protein

DIC: Differential interference contrast

EC: Endothelial cells

Gal: Galactose α-1,3-galactose

GalTKO: α-1,3-galactosyl-transferase knockout

HUVEC: Human umbilical vein endothelial cells

LED: Light-emitting diode

MDCK: Madin-Darby Canine Kidney

NIR: Near-infrared

OBM: Oblique back-illumination microscopy

OPL: Optical path length

PAOEC: porcine aortic endothelial cells

PC: Phase contrast

RBC: Red blood cell

WT: Wild type

References

American Journal of Transplantation. (2016). OPTN/SRTR Annual Data Report 2014. *American Journal of Transplantation, 16*(S2), 4-7.

Arnison, M. R., Larkin, K. G., Sheppard, C. J., Smith, N. I., & Cogswell, C. J. (2004). Linear phase imaging using differential interference contrast microscopy. *Journal of Microscopy, 214*(1), 7-12.

Burdorf, L., Stoddard, T., Zhang, T., Rybak, E., Riner, A., Avon, C., . . . Pierson, R. (2014). Expression of Human CD46 Modulates Inflammation Associated With GalTKO Lung Xenograft Injury (. *American Journal of Transplantation, 14*(5), 1084-1095.

Callamaras, N., & Parker, I. (1999). Construction of a confocal microscope for real-time x-y and x-z imaging. *Cell Calcium, 26*(6), 271-279.

Conant, C., Schwartz, M. A., Beecher, J. E., Rudoff, R. C., Ionescu-Zanetti, C., & Nevill, J. (2011). Well plate microfluidic system for investigation of dynamic platelet behavior under variable shear loads. *Biotechnology and Bioengineering, 108*(12), 2978-2987.

Cox, G., & Sheppard, C. J. (2004). Practical limits of resolution in confocal and non-linear microscopy. *Microscopy Research and Technique, 63*(1), 18-22.

Ekser, B., Ezzelarab, M., Hara, H., van der Windt, D. J., Wijkstrom, M., Bottino, R., . . . Cooper, D. K. (2012). Clinical xenotransplantation: the next medical revolution? *The Lancet, 379*, 672-683.

Ford, T. N., & Mertz, J. (2013). Video-rate imaging of microcirculation with single-exposure oblique back- illumination microscopy. *Journal of Biomedical Optics, 18*(6).

Ford, T., Chu, K., & Mertz, J. (2012). Phase-gradient microscopy in thick tissue with oblique back-illumination. *Nat Meth, 9*(12), 1195-1197.

Harris, D. G., Benipal, P. K., Cheng, X., Burdorf, L., Azimzadeh, A. M., & Pierson, III, R. N. (2015). Four-Dimensional Characterization of Thrombosis in a Live-Cell, Shear-Flow Assay: Development and Application to Xenotransplantation. *PLoS ONE , 10*(4).

Huang, B., Bates, M., & Zhuang, X. (2009). Super resolution fluorescence microscopy (article) Author. *Annual review of biochemistry, 78*, 993-1016.

ibidi GmbH. (2016, March). *Application Note 11*. Retrieved from Ibidi: http://ibidi.com/fileadmin/support/application_notes/AN11_Shear_stress.pdf

Kickler, K., Maltby, K., Choileain, S. N., Stephen, J., Wright, S., Hafler, D. A., . . . astier, A. L. (2012). Prostaglandin E2 affects T cell responses through modulation of CD46 expression(). *Journal of Immunology, 188*(11), 5303-5310.

Klymiuk, N., Aigner, B., Brem, G., & Wolf, E. (2010). Genetic modification of pigs as organ donors for xenotransplantation. *Molecular Reproduction and Development, 77*(3), 209-221.

Lang, W. (1982). *Nomarski differential interference-contrast microscopy*. Oberkochen, Carl Zeiss .

Litwin, M. S., & Chapman, K. (1970). Physical factors affecting human blood viscosity. *Journal of Surgical Research, 10*(9), 433-436.

McCurry, K. R., Kooyman, D. L., Alvarado, C. G., Cotterell, A. H., Martin, M. J., Logan, J. S., & Platt, J. L. (1995). Human complement regulatory proteins protect swine-to-primate cardiac xenografts from humoral injury. *Nat Med, 1*(5), 423-427.

Mertz, J. (2009). *Introduction to Optical Microscopy* . W.H. Freeman.

Mukovozov, I., Huang, Y.-W., Zhang, Q., Liu, G., Siu, A., Sokolskyy, Y., . . . Robinson, L. A. (2015). The Neurorepellent Slit2 Inhibits Postadhesion Stabilization of Monocytes Tethered to Vascular Endothelial Cells. *The Journal of Immunology, 195*(7), 3334-3344.

Ockenga, W. (2011). *Phase Contrast: Making Unstained Phase Objects Visible*. Retrieved from Science Lab: http://www.leica-microsystems.com/science-lab/phase-contrast/

Pierson, R. N., Dorling, A., Ayares, D., Michael, R. A., Seebach, J. D., Fishman, J. A., . . . Cooper, D. K. (2009). Current status of xenotransplantation and prospects for clinical application. *Xenotransplantation, 16*(5), 263-280.

Prabhakarpandian, B., Shen, M.-C., Pant, K., & Kiani, M. F. (2011). Microfluidic devices for modeling cell--cell and particle--cell interactions in the microvasculature. *Microvascular Research, 82*(3), 210-220.

Rosenthal, C. K. (2009). Contrast by interference. *Nature Milestones: Light Microscopy*.

Schroeder, C., Allan, J. S., Nguyen, B. N., Wu, G., Zhang, T., Azimzadeh, A. M., . . . Pierson III, R. N. (2005). Transplantation Proceedings. *Hyperacute rejection is attenuated in GalT knockout swine lungs perfused ex vivo with human blood, 37*(1), 512-513.

Smith, S. (2013). *Digital Signal Processing: A Practical Guide for Engineers and Scientists*. Newnes.

Van Kruchten, R., Cosemans, J. M., & Heemskerk, J. W. (2012). Measurement of whole blood thrombus formation using parallel-plate flow chambers -- a practical guide. *Platelets, 23*(3), 229-242.

Wang, G., & Li, Y. (1999). Axiomatic Approach for Quantification of Image Resolution. *IEEE Signal Processing Letters*.

Yurkin, M. A., Semyanov, A. K., Tarasov, P. A., Chernyshev, A. V., Hoekstra, A. G., & Maltsev, V. P. (2005). Experimental and theoretical study of light scattering by individual mature red blood cells by use of scanning flow cytometry and a discrete dipole approximation. *Appl. Opt. , 44*(25), 5249-5256.

Zavislan, J. M. (2009). Design of reflectance confocal microscopes for clinical applications. *Proc. SPIE, 7170*.